Bulletin of Earthquake Engineering (2024) 22:2105–2138
https://doi.org/10.1007/s10518-023-01850-4

ORIGINAL ARTICLE

The evaluation of target displacement in structural systems using damage-based N_2 (DN_2) method under far-field ground motions for performance-based design theory

Rasool Nodeh Farahani[1] · **Gholamreza Abdollahzadeh**[1] · **Alireza Mirza Goltabar Roshan**[1]

Received: 9 April 2023 / Accepted: 21 December 2023 / Published online: 20 January 2024

Abstract
The aim of this paper is based on the simple nonlinear procedure founded on the Park-Ang damage index model at different constant damage levels to evaluate the target displacement and performance point (P.P.). The mentioned procedure represents the intersection of the pushover capacity curve with the seismic hazard demand curve according to the equivalent period of vibration and damping in ADRS format. Hence, the damage-based response acceleration ratio is determined at different damage levels and periods for developing inelastic spectra from elastic ones. Then, the relation between the strength reduction factor (R-factor) and damage was extended at different damage levels and periods of vibration to predict the target displacement at the desired damage level, known as the performance point. It is worth mentioning that the cited procedure is represented for four hysteresis models, including Elastic-Perfectly-Plastic (EPP), Modified Clough (MC), moderate stiffness-strength deterioration (MSD), and severe stiffness-strength deterioration (SSD) models, to consider the theory for well-design and not well-designed systems in both steel and concrete structures. The mentioned procedure is the N_2 theory development based on the damage model called the DN_2 method in this investigation. Two experimental reinforced concrete bridge piers and three steel moment resisting frame structures with different periods, from low to high duration, are considered to verify the suggested procedure. Statistical results show that the target displacement and P.P. are evaluated appropriately regarding presented equations and proposed methodology compared to previous studies.

Keywords Damage · Target displacement · Performance point · Capacity · Demand

✉ Gholamreza Abdollahzadeh
abdollahzadeh@nit.ac.ir

[1] Civil Engineering Faculty, Babol Noshirvani University of Technology, Babol, Iran

1 Introduction

Predicting target displacement at the desired performance level is one of the main issues in performance-based earthquake engineering (PBEE). The estimation of target displacement is used in pushover analysis to push the structure up to the desired performance level for evaluation of structural status in permeance-based design theory. Hence, different estimation methodologies have been proposed by many researchers to estimate the nonlinear target displacement in structural systems. One of the simple methods, which includes the estimation of maximum nonlinear displacement from the maximum linear displacement of the single-degree-of-freedom (SDOF) system with constant damping and period of vibration, has been presented by Veletsos and Newmark (1960) and Veletsos et al. (1965). The mentioned method was comprehensively developed by Miranda and his colleagues (1991, 1994; Miranda 1993, 2000, 2001; Baez and Miranda 2000; Ruiz-García and Miranda 2003, 2004, 2006, 2007) as an inelastic displacement ratio (IDR). The inelastic displacement ratio is available as the coefficient method in seismic codes, such as FEMA-273 (1997), FEMA-356 (2000), FEMA-440 (2005), and ASCE/SEI 41–17 (2017). The capacity spectrum method, known as CSM, has been adopted by the ATC-40 (1996) code for retrofitting and evaluating reinforced concrete structures using the effective damping ratio and period of vibration (Fajfar 1999; Lin and Chang 2003). The energy balance was introduced by Leelataviwat et al. from 1999 to 2009 (Leelataviwat et al. 1999, 2002, 2007, 2009) based on the intersection of energy demand and capacity to estimate probable nonlinear displacement for use in plastic-based performance design (PBPD) (Goel et al. 2010; Liao and Goel 2014). The N_2 method was first introduced by Fajfar and Fischinger (1988) for regular RC frame systems to estimate nonlinear target displacement based on the intersection of capacity and demand curves. The N_2 method was developed by Fajfar and Gaspersc (1996) to evaluate the structural performance point using the first vibration mode. The proposed procedure, founded by Fajfar, was formulated comprehensively, and the influence of higher vibration modes was considered in this methodology (Fajfar 2000). It is worth mentioning that the N_2 method is applicable to complex structures (Kreslin and Fajfar 2010) and could be used for seismic evaluation of existing and new buildings (Kilar and Fajfar 1997). Additionally, one of the main features of this method is its ability to be used for all kinds of structural systems, such as asymmetric buildings (Dolšek and Fajfar 2007), infill reinforced concrete frames, structural systems with torsional effects (Bhatt and Bento 2011), and others. The mentioned procedure was extended considering higher modes (Kreslin and Fajfar 2010, 2011, 2012) and the N_2 multi-mode procedure (NMP) by Zarrin et al. (2021).

It is worth mentioning that the N_2 method has been represented according to the R-μ-T relationship to evaluate the target displacement. However, the cited method can be extended for damage-based evaluation and design of structures at the desired damage level (Amirchoupani et al. 2023a, b; Farahani et al. 2023). For example, Zhai et al. (2013a, b) developed the IDR for SDOF systems based on the Park-Ang damage index model (Park and Ang 1985) under far-field and mainshock-aftershock ground motions at different constant damage levels and periods of vibration. Moreover, Wen et al. (2014) extended the damage-based IDR for near-field pulse-like records as dangerous earthquakes for ordinary buildings. Recently, Amirchoupani et al. (2023a, b) proposed the damage-based IDR based on hysteresis to input energy intensity to predict target displacement in coefficient method theory, although it could only be applicable to the performance-based design. Although different damage models have been suggested before by many researchers (Powell and Allahabadi 1988; Kraetzig et al. 1989; Kunnath et al. 1997; Ghobarah et al. 1999; Diaz

et al. 2017; Su et al. 2017; Mahboubi and Shiravand 2019a, b; Amirchoupani et al. 2021), the Park-Ang damage model is one of the popular indices for assessing damage in structural elements.

The N_2 method is developed in this investigation regarding the well-known damage-based Park-Ang model called the DN_2 procedure under far-field earthquake ground motions. Unlike the N_2 method, which is only based on ductility, the presented theory can consider the influence of hysteresis energy as a principal cause of failure in structural systems, frequency content, and the ultimate displacement of the structural system to estimate the structural status and target displacement. The damage-based N_2 procedure (DN_2) can be used in the energy-based design approach and gives a particular insight into structural behavior. Hence, the damage-based response acceleration ratio for developing inelastic spectra from elastic values and the relation between the strength reduction factor (R-factor) and damage is determined at different damage levels, periods of vibration, and hysteresis models (EPP, MC, MSD, SSD) to estimate target displacement and performance point. Moreover, mathematical equations are suggested for computing the damage-based response acceleration ratio and the R-DI-T relation using least-square nonlinear regression analysis. Two empirical reinforced concrete bridge piers with analytical verification and three designed steel resisting moment structures were adopted to verify the proposed methodology from low- to high-period duration. Statistical results show that the suggested procedure can estimate the performance point and target displacement appropriately, especially in short-period regions, compared to the coefficient method proposed by other researchers.

2 Earthquake ground motions

In this paper, 105 earthquake ground motion pairs, including 210 records from worldwide, were selected for performing nonlinear time history analysis. The earthquake ground motions from far-field sources were chosen in three categories, including 35 pairs recorded on sites with the shear velocity of 750 m/s to 1500 m/s, 365 m/s to 750 m/s, and 185 m/s to 365 m/s, respectively. Based on ASCE/SEI 7 (ASCE/SEI 7–10 2010; ASCE/SEI 7–16 2016), the mentioned categories are known as soil classes B, C, and D, respectively. It is necessary to explain that the recorded ground motions in soft soil sites (E and F soil classes) and pulsive ones are not in the scope of this investigation. The earthquake ground motions were selected from the Pacific Earthquake Engineering Research Center (PEER) from Shallow Crustal Earthquakes in Active Tectonic Regimes in the NGA/WEST 2 project. Tables 1, 2, 3 illustrates the selected ground motion characteristics, including RSN number, event year, earthquake name, station name, moment magnitude (M_w), fault mechanism, Joyner-Boore distance, rapture distance, shear wave velocity, and peak ground acceleration in two horizontal components. The following criterion was considered in ground motion selection:

The earthquake ground motions were chosen from (1) recorded data with higher than $M_w = 5.5$ moment magnitude. The mentioned criteria were selected because the nonlinear behavior of structures in lower values is not probable, and lower values cannot expose the structures to higher risks. (2) recorded data with Joyner-Boore distance (Boore et al. 1997) lower than 80 km. (3) recorded data on free-field, where the influence of soil-structure interaction is not prominent. (4) data with available records in two horizontal directions. (5) recorded data with peak ground acceleration higher than 40 cm/s^2.

Table 1 Soil class A, B earthquake ground motions

RSN	Year	Earthquake name	Station name	Mw	Mechanism	Rjb (km)	Rrup (km)	Vs30 (m/sec)	PGA-1 (m/s^2)	PGA-2 (m/s^2)
80	1971	San Fernando	Pasadena	6.6	Reverse	21.5	21.5	969.07	93.5	200.9
146	1979	Coyote Lake	Gilroy Array #1	5.7	Strike slip	10.21	10.67	1428.14	92.2	114.4
455	1984	Morgan Hill	Gilroy Array #1	6.1	Strike slip	14.9	14.91	1428.14	68.3	96.9
680	1987	Whittier Narrows	Pasadena	5.9	Reverse Oblique	6.78	18.12	969.07	109.6	92.9
703	1987	Whittier Narrows	Vasquez Rocks Park	5.9	Reverse Oblique	47.25	50.39	996.43	60.7	64.5
765	1989	Loma Prieta	Gilroy Array #1	6.9	Reverse Oblique	8.84	9.64	1428.14	407.3	475.4
788	1989	Loma Prieta	Piedmont Jr High Sch	6.9	Reverse Oblique	72.9	73	895.36	82.1	70.2
789	1989	Loma Prieta	Point Bonita	6.9	Reverse Oblique	83.37	83.45	1315.92	70.3	72.1
795	1989	Loma Prieta	SF-Pacific Heights	6.9	Reverse Oblique	75.96	76.05	1249.86	60.8	46.6
797	1989	Loma Prieta	SF-Rincon Hill	6.9	Reverse Oblique	74.04	74.14	873.1	77.3	91.1
804	1989	Loma Prieta	So. San Francisco	6.9	Reverse Oblique	63.03	63.15	1020.62	53.1	103.1
1011	1994	Northridge	LA-Wonderland Ave	6.6	Reverse	15.11	20.29	1222.52	101.3	155.9
1091	1994	Northridge	Vasquez Rocks Park	6.6	Reverse	23.1	23.64	996.43	148.1	136.4
1108	1995	Kobe	Kobe University	6.9	Strike slip	0.9	0.92	1043	270.5	305.8
1613	1999	Duzce	Lamont 1060	7.1	Strike slip	25.78	25.88	782	52.0	24.8
1649	1991	Sierra Madre	Vasquez Rocks Park	5.6	Reverse	37.63	39.81	996.43	96.0	122.9
2753	1999	Chi-Chi	CHY102	6.2	Strike slip	39.3	39.32	804.36	57.8	52.3
2989	1999	Chi-Chi	CHY102	6.2	Reverse	69.76	74.16	804.36	63.0	56.2
3251	1999	Chi-Chi	TTN042	6.2	Reverse	84.68	85.17	845.34	58.4	43.2
3925	2000	Tottori	OKYH07	6.6	Strike slip	15.23	15.23	940.2	125.3	181.1
3954	2000	Tottori	SMNH10	6.6	Strike slip	15.58	15.59	967.27	226.2	155.5
4083	2004	Parkfield	PARKFIELD	6.0	Strike slip	4.66	5.29	906.96	240.6	192.3
4167	2004	Niigata	FKSH07	6.6	Reverse	52.15	52.3	828.95	96.0	140.4
4312	1984	Umbria	Gubbio	5.6	Normal	14.67	15.72	922	49.1	66.1

Table 1 (continued)

RSN	Year	Earthquake name	Station name	Mw	Mechanism	Rjb (km)	Rrup (km)	Vs30 (m/sec)	PGA-1 (m/s^2)	PGA-2 (m/s^2)
5483	2008	Iwate	AKTH05	6.9	Reverse	37.45	39.41	829.46	65.1	83.4
5618	2008	Iwate	IWT010	6.9	Reverse	16.26	16.27	825.83	283.1	221.2
5646	2008	Iwate	IWTH14	6.9	Reverse	99.04	99.05	816.31	130.1	170.7
5649	2008	Iwate	IWTH17	6.9	Reverse	72.44	72.44	1269.78	58.7	59.1
5650	2008	Iwate	IWTH18	6.9	Reverse	64.27	64.27	891.55	137.6	132.4
5655	2008	Iwate	IWTH23	6.9	Reverse	68.03	68.03	922.89	105.4	116.5
5670	2008	Iwate	MYG011	6.9	Reverse	82.93	82.93	1423.8	56.0	81.3
5679	2008	Iwate	MYGH03	6.9	Reverse	56.72	56.72	933.96	91.2	80.3
5680	2008	Iwate	MYGH04	6.9	Reverse	40.42	40.43	849.83	149.5	223.0
5685	2008	Iwate	MYGH11	6.9	Reverse	57.15	57.15	859.19	119.4	180.9
8167	2003	San Simeon	Diablo Canyon	6.5	Reverse	37.92	37.97	1100	45.6	33.7

Table 2 Soil class C earthquake ground motions

RSN	Year	Earthquake name	Station name	Mw	Mechanism	Rjb (km)	Rrup (km)	Vs30 (m/sec)	PGA-1 (m/s^2)	PGA-2 (m/s^2)
57	1971	San Fernando	Castaic-old ridge route	6.6	Reverse	19.33	22.63	450.28	314.4	269.9
125	1976	Friuli	Tolmezzo	6.5	Reverse	14.97	15.82	505.23	350.3	309.1
139	1978	Tabas	Dayhook	7.3	Reverse	0	13.94	471.53	317.7	401.6
231	1980	Mammoth lakes	Long valley dam	6.0	Normal oblique	12.56	15.46	537.16	422.1	266.2
250	1980	Mammoth lakes	Long valley dam	5.9	Strike slip	9.65	16.03	537.16	927.3	405.9
265	1980	Victoria	Cerro Prieto	6.3	Strike slip	13.8	14.37	471.53	633.1	620.5
448	1984	Morgan Hill	Anderson dam	6.1	Strike slip	3.22	3.26	488.77	414.8	283.9
496	1985	Nahanni	Site 2	6.7	Reverse	0	4.93	605.04	509.3	348.3
564	1986	Kalamata	Kalamata	6.2	Normal	6.45	6.45	382.21	234.1	267.2
589	1987	Whittier Narrows	Alhambra-Fremont School	5.9	Reverse oblique	1.67	14.66	549.75	284.2	380.1
690	1987	Whittier Narrows	San Gabriel-E Grand Ave	5.9	Reverse oblique	0	15.2	401.37	257.3	208.5
755	1989	Loma Prieta	Coyote Lake Dam	6.9	Reverse oblique	19.97	20.34	561.43	149.0	475.5
787	1989	Loma Prieta	Palo Alto–SLAC Lab	6.9	Reverse oblique	30.62	30.86	425.3	191.1	271.9
801	1989	Loma Prieta	San Jose–Santa Teresa Hills	6.9	Reverse oblique	14.18	14.69	671.77	271.1	253.9
1012	1994	Northridge	LA 00	6.6	Reverse	9.87	19.07	706.22	258.0	374.6
1512	1999	Chi-Chi	TCU078	7.6	Reverse oblique	0	8.2	443.04	438.8	301.1
1521	1999	Chi-Chi	TCU089	7.6	Reverse oblique	0	9	671.52	346.6	225.0
1787	1999	Hector Mine	Hector	7.1	Strike slip	10.35	11.66	726	260.4	322.0
2627	1999	Chi-Chi	TCU076	6.2	Reverse	13.04	14.66	614.98	511.7	158.0
2628	1999	Chi-Chi	TCU078	6.2	Reverse	0	7.62	443.04	439.0	266.0
4031	2003	San Simeon	Templeton-1-story Hospital	6.5	Reverse	5.07	6.22	410.66	426.9	473.3
4130	2004	Parkfield-02	Parkfield-Vineyard Cany 1E	6.0	Strike slip	1.59	2.96	381.27	263.3	284.2
4141	2004	Parkfield-02	PARKFIELD–UPSAR 05	6.0	Strike slip	9.14	9.61	440.59	360.3	235.3
4143	2004	Parkfield-02	PARKFIELD–UPSAR 07	6.0	Strike slip	9.14	9.61	440.59	319.7	368.4

Table 2 (continued)

RSN	Year	Earthquake name	Station name	Mw	Mechanism	Rjb (km)	Rrup (km)	Vs30 (m/sec)	PGA-1 (m/s^2)	PGA-2 (m/s^2)
4147	2004	Parkfield-02	PARKFIELD–UPSAR 11	6.0	Strike slip	8.93	9.41	466.12	456.8	350.0
4213	2004	Niigata	NIG023	6.6	Reverse	25.33	25.82	654.76	274.9	397.0
4229	2004	Niigata	NIGH12	6.6	Reverse	9.93	10.72	564.25	343.4	409.5
4481	2009	L'Aquila	L'Aquila-V. Aterno	6.3	Normal	0	6.81	685	472.4	507.1
4846	2007	Chuetsu-oki	Joetsu Yanagishima	6.8	Reverse	28.07	31.43	605.71	275.4	319.6
4864	2007	Chuetsu-oki	Yoitamachi Yoita	6.8	Reverse	4.69	16.1	655.45	312.6	278.6
4873	2007	Chuetsu-oki	Kashiwazaki City	6.8	Reverse	10.38	20.03	561.59	355.2	713.0
5286	2007	Chuetsu-oki	NIGH13	6.8	Reverse	29.84	33.57	461.1	168.3	270.4
5478	2008	Iwate	AKT023	6.9	Reverse	11.68	16.96	555.96	358.8	360.9
5656	2008	Iwate	IWTH24	6.9	Reverse	3.1	5.18	486.41	429.8	508.7
8486	2004	Parkfield-02	Hog Canyon	6.0	Strike slip	4.51	5.28	376	270.8	253.9

Table 3 Soil class D earthquake ground motions

RSN	Year	Earthquake name	Station name	Mw	Mechanism	Rjb (km)	Rrup (km)	Vs30 (m/sec)	PGA-1 (m/s^2)	PGA-2 (m/s^2)
95	1972	Managua	Managua-ESSO	6.24	Strike slip	3.51	4.06	288.77	364.8	323.3
174	1979	Imperial Valley	El Centro Array #11	6.53	Strike slip	12.56	12.56	196.25	359.8	372.2
183	1979	Imperial Valley	El Centro Array #8	6.53	Strike slip	3.86	3.86	206.08	598.5	457.2
322	1983	Coalinga	Cantua Creek School	6.36	Reverse	23.78	24.02	274.73	221.1	283.0
367	1983	Coalinga	Pleasant Valley P.P.-bldg	6.36	Reverse	7.69	8.41	257.38	294.6	266.7
614	1987	Whittier Narrows	Downey-Birchdale	5.99	Reverse oblique	14.9	20.79	245.06	227.3	341.6
700	1987	Whittier Narrows	Tarzana-Cedar Hill	5.99	Reverse oblique	38.24	41.22	257.21	463.0	587.4
725	1987	Superstition Hills	Poe Road (temp)	6.54	Strike slip	11.16	11.16	316.64	466.0	280.7
776	1989	Loma Prieta	Hollister-South & Pine	6.93	Reverse oblique	27.67	27.93	282.14	362.9	175.3
778	1989	Loma Prieta	Hollister Differential Array	6.93	Reverse oblique	24.52	24.82	215.54	263.8	273.3
783	1989	Loma Prieta	Oakland-Outer Harbor	6.93	Reverse oblique	74.16	74.26	248.62	284.7	265.5
799	1989	Loma Prieta	SF Intern. Airport	6.93	Reverse oblique	58.52	58.65	190.14	231.4	324.1
848	1992	Landers	Coolwater	7.28	Strike slip	19.74	19.74	352.98	278.3	409.3
949	1994	Northridge	Arleta-Nordhoff Fire Sta	6.69	Reverse	3.3	8.66	297.71	338.5	301.9
995	1994	Northridge	LA-Hollywood Stor FF	6.69	Reverse	19.73	24.03	316.46	227.0	351.5
998	1994	Northridge	LA-N Westmoreland	6.69	Reverse	23.4	26.73	315.06	424.0	326.7
999	1994	Northridge	LA-Obregon Park	6.69	Reverse	35.43	37.36	349.43	347.9	551.9
1082	1994	Northridge	Sun Valley-Roscoe Blvd	6.69	Reverse	5.59	10.05	320.93	271.4	438.7
1101	1995	Kobe	Amagasaki	6.9	Strike slip	11.34	11.34	256	270.5	320.6
1141	1995	Dinar	Dinar	6.4	Normal	0	3.36	219.75	320.1	273.3
3749	1992	Cape Mendocino	Fortuna fire station	7.01	Reverse	16.54	20.41	355.18	326.6	277.7
4108	2004	Parkfield	Parkfield-fault zone 3	6	Strike slip	1.1	2.73	211.74	371.7	393.9
4112	2004	Parkfield	Parkfield-fault zone 8	6	Strike slip	3.05	3.95	308.84	563.1	479.4
4207	2004	Niigata	NIG017	6.63	Reverse	4.22	12.81	274.17	370.9	467.3

Table 3 (continued)

RSN	Year	Earthquake name	Station name	Mw	Mechanism	Rjb (km)	Rrup (km)	Vs30 (m/sec)	PGA-1 (m/s^2)	PGA-2 (m/s^2)
4861	2007	Chuetsu-oki	Nakanoshima Nagaoka	6.8	Reverse	10.73	19.89	319	319.0	344.9
4866	2007	Chuetsu-oki	Kawanishi Izumozaki	6.8	Reverse	0	11.75	338.32	317.4	349.9
4875	2007	Chuetsu-oki	Kariwa	6.8	Reverse	0	12	282.57	353.1	465.9
4896	2007	Chuetsu-oki	Kashiwazaki NPP	6.8	Reverse	0	10.97	201	436.0	345.9
5664	2008	Iwate	MYG005	6.9	Reverse	10.71	13.47	361.24	525.3	437.1
5814	2008	Iwate	Furukawa Osaki City	6.9	Reverse	31.07	31.08	248.19	312.1	232.0
5836	2010	El Mayor	El Centro-Meloland Geot	7.2	Strike slip	28.53	29	264.57	285.8	430.9
6877	1992	Joshua Tree	Indio-Jackson Road	6.1	Strike slip	25.04	25.53	292.12	399.3	205.8
6893	2010	Darfield	DFHS	7	Strike slip	11.86	11.86	344.02	462.6	502.9
6923	2010	Darfield	Kaiapoi North School	7	Strike slip	30.53	30.53	255	352.8	295.7
8067	2011	Christchurch	Christchurch Cashmere	6.2	Reverse oblique	4.44	4.46	204	392.8	342.4

2.1 Methodology

As mentioned before, the DN_2 methodology, known as the damage-based N_2 procedure, was extended for performance-based design and evaluation of structures. As cited in the literature, the extent of the damage model in the N_2 theory can predict structural performance more intuitively. As explained before, the Park-Ang damage model was used in this investigation for developing the N_2 procedure, reference to Eq. (1), given as:

$$DI = \frac{x_m - x_y}{x_u - x_y} + \beta \frac{E_h}{x_u F_y} = \frac{\mu_m - 1}{\mu_u - 1} + \beta \frac{E_h}{\mu_u F_y x_y} \tag{1}$$

where x_m is the maximum displacement of the system, x_y is the yield displacement, x_u is the ultimate displacement of the system, E_h is the hysteresis energy, F_y is the yield force of the system, μ_m is the ductility of the system, μ_u is the ultimate ductility of the system, and β is constant parameter defined by experiment and guesswork.

Park-Ang proposed a formula to determine the β coefficient, but the scatter among data was too large. The experimental works illustrate that the value of β coefficient is between − 0.3 to about 1.2 with a median of 0.15 in investigations. Moreover, Zhai et al. (2013b) confirmed that the influence of β coefficient is below 20 percent in short-period regions and lower in long periods. The cited result was confirmed by other researchers, such as Decanini et al. (2004), Panyakapo (2004), Wen et al. (2014), and Amirchoupani et al. (2023a, b). Hence, the β=0.15 was considered for hysteresis energy calibration in this research paper.

Park-Ang (1985) categorized their damage model into five bounds, including no damage with no cracking, minor damage with light cracks, moderate damage with severe cracking and spalling of concrete cover, severe damage with crushing concrete core and exposure of rebars in the elements, and total collapse of the system, as presented in Table 4. Seven steps in DN_2 methodology are needed for predicting the performance point and damage level in structural models, which are explained in detail, given as:

Step 1: In the first step, structural data and linear acceleration spectrum must be defined due to the desired seismic hazard level, as illustrated in Fig. 1. The vertical axis in the elastic acceleration spectrum curve is acceleration responses, and the horizontal axis is the natural period. The T_c and T_D in the figure represent the end of the acceleration- and velocity-sensitive regions, respectively.

Step 2: In the second step, the acceleration spectrum must be converted to acceleration-displacement (AD) format for elastic SDOF systems, according to given equation:

$$S_{de} = \frac{T^2}{4\pi^2} S_{ae} \tag{2}$$

Table 4 Park-Ang damage model category (Park and Ang 1985)

NO	Damage index	Damage description
1	DI < 0.10	No damage and minor cracking
2	0.10 ≤ DI < 0.25	Minor damage, light cracks
3	0.25 ≤ DI < 0.40	Moderate damage, severe cracking and spalling
4	0.40 ≤ DI < 1.0	Severe damage, crushing of concrete and rebars expose
5	DI ≥ 1.0	Total collapse

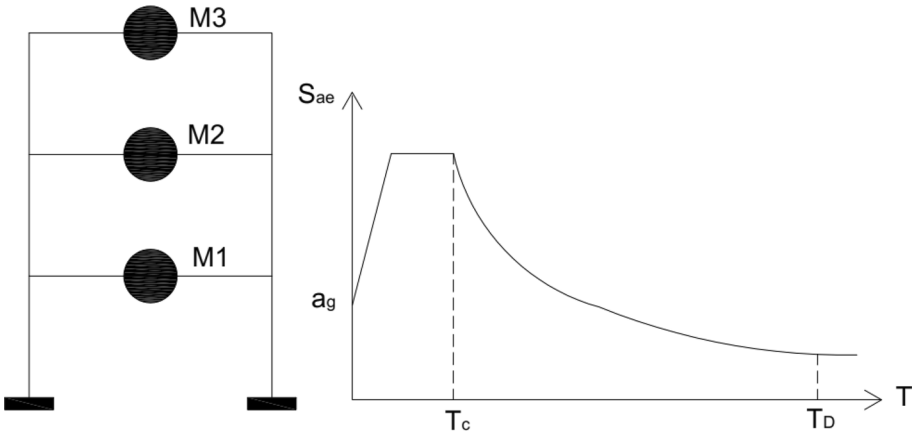

Fig. 1 Structural data and elastic acceleration spectrum

where T is the fundamental period of vibration, and S_{ae} is the elastic response acceleration.

Step 3: The damage-based inelastic acceleration spectrum curve must be determined in the third step. Hence, the damage-based inelastic response accelerations regarding the Park-Ang damage model were computed at 30 periods of vibration from 0.1 to 3s, with a 0.1 time-step and four damage levels, including 0.1, 0.25, 0.4, and 0.8, respectively. The considered damage levels are according to the Park-Ang limit states presented in Table 4. It is worth mentioning that damage higher than 0.8 was not considered in this study because higher values expose the structure to probable collapse conditions, and this is not an appropriate status in performance-based design theory. Therefore, the inelastic acceleration spectrum ratio was extended as the proportion of maximum inelastic acceleration to maximum elastic one at four damage levels to obtain the inelastic response acceleration from elastic one at the desired damage level. As illustrated in Fig. 2, the input ground motion, hysteresis model, period of vibration, damping ratio, structural stiffness, mass, ultimate ductility of the system, β coefficient, and target damage level were defined to perform linear and nonlinear time history analysis for achieving elastic (S_{ae}) and inelastic (S_a) response accelerations. The yield strength of the SDOF system is equal to $Fy = m.S_{ae}$, where m is the mass of the SDOF system. Then, the system strength was decreased gradually, and the damage was calculated at each strength level by try and error procedure with less than 1% error. When the computed damage index reached the target value (with a lower than 1% error), the nonlinear response acceleration was utilized as the desired data. Therefore, the response acceleration ratio was calculated as nonlinear to linear response acceleration proportion to predict the inelastic values from elastic ones. The cited procedure was repeated for 30 periods of vibration, four damage levels, four hysteresis models, three ultimate ductility from 4 to 8, and 210 far-field ground motions by performing 302,400 nonlinear time history analysis. The OpenSEES version 3.0.3 and MATLAB 2017 software were used for carrying out linear and nonlinear dynamic analysis and post-processing data, respectively.

As noted previously, four hysteresis models were used to compute damage-based response acceleration ratios, including Elastic-Perfectly-Plastic (EPP), Modified Clough (MC), moderate stiffness deterioration and strength degradation (MSD), and severe stiffness deterioration and strength degradation (SSD). The mentioned hysteresis models are conventional structural behaviors adapted in the FEMA series (FEMA 273 1997, 2005;

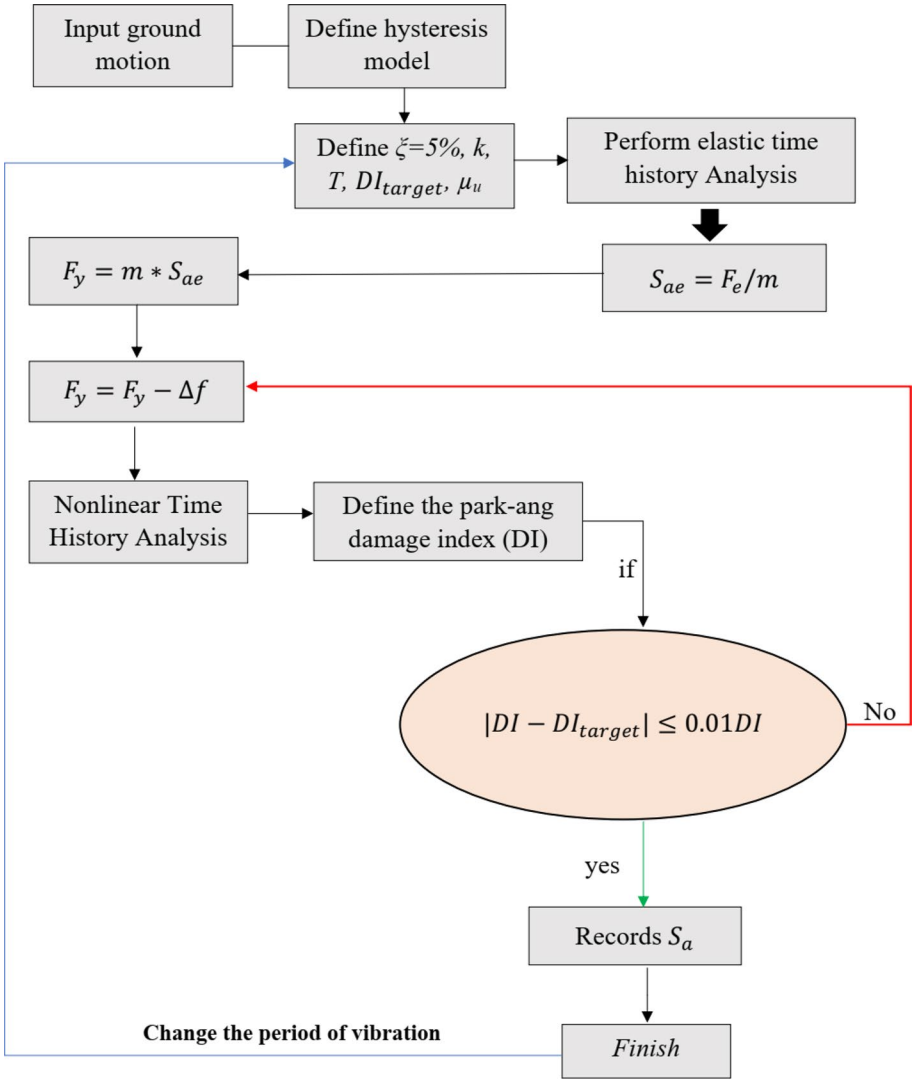

Fig. 2 The procedure of damage-based response spectrum calculation

FEMA 356 2000), ASCE/SEI 41–17 (2017), and other research studies. The EPP is a popular hysteresis model for simulating the steel structure behavior, and the MC, MSD, and SSD are used to model the concrete structure behaviors. The high stiffness deterioration and strength degradation in concrete structures are generally related to not well-designed systems with high bar slippage, bond-slip behavior, cracking, and spalling of concrete during seismic excitation. Figure 3 shows the EPP, MC, MSD, and SSD hysteresis models used in this investigation under SAC standard loading protocols.

Figure 4a illustrates the S_a/S_{ae}-T spectrum (response acceleration ratio) at different periods of vibration and damage levels. The S_a/S_{ae} values are decreased by increasing the damage level. However, S_a/S_{ae} values become constant at middle period ranges, where the nonlinear response acceleration is approximately equal to linear ones. Moreover, the

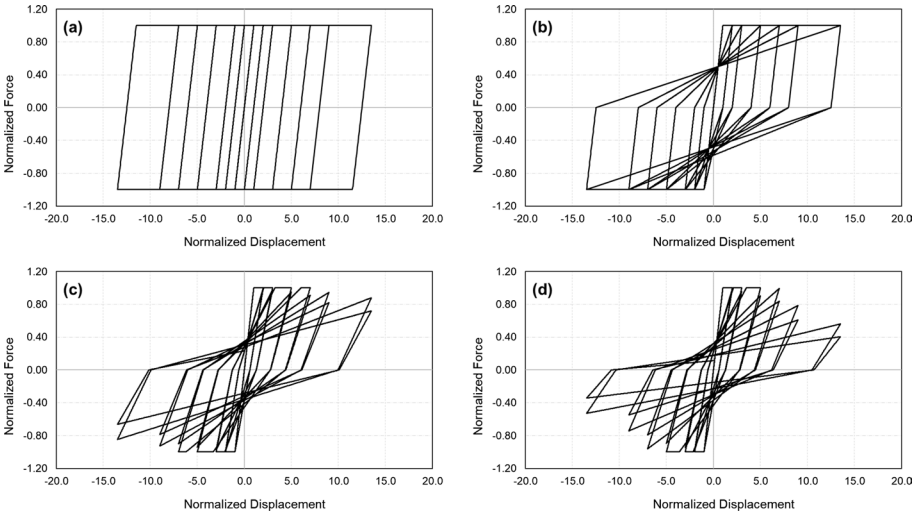

Fig. 3 The hysteresis models, including **a** EPP **b** MC **c** MSD **d** SSD

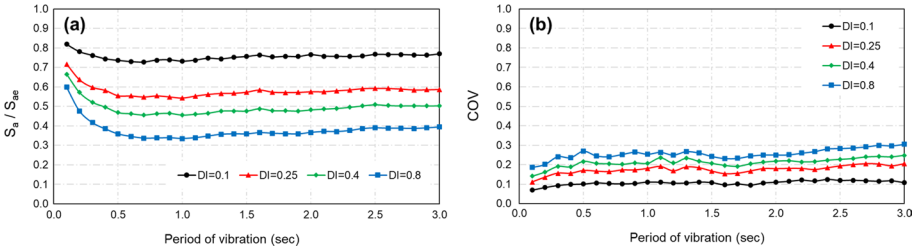

Fig. 4 The mean and coefficient of variation in response acceleration ratio for $\mu_u = 6$

coefficient of variation (COV) among data at different damage levels is not affected by the period of vibration, especially in the short-period region, reference to Fig. 4b. The COV at each damage level is not high, and it helps to have a robust equation to estimate the S_a in different strength levels, especially in higher damage levels where the dispersion among data increases. It is necessary to explain that Fig. 4 is only presented for $\mu_u = 6$ due to the space limitation of the paper. However, the illustrated trend was observed in other ultimate ductility factors.

The influence of the ultimate ductility of the system on the damage-based response acceleration ratio is illustrated in Fig. 5. Figure 5 shows that the differences between response acceleration ratios at each damage level increased by increasing the ultimate ductility of the system. The mentioned trend is amplified in higher damage levels (about 30%), where damage is 0.4 and 0.8. Therefore, the influence of the ultimate ductility on response acceleration ratios is prominent, and this parameter should be considered in the proposed formula.

A simplified equation based on the S_a/S_{ae}-DI-T relation was proposed according to the achieved results for estimating the response acceleration ratio at the desired damage level, with reference to Eq. (3). Table 5 presents the constant parameters in Eq. (3) obtained from the mean of the inelastic response acceleration ratio by conducting the

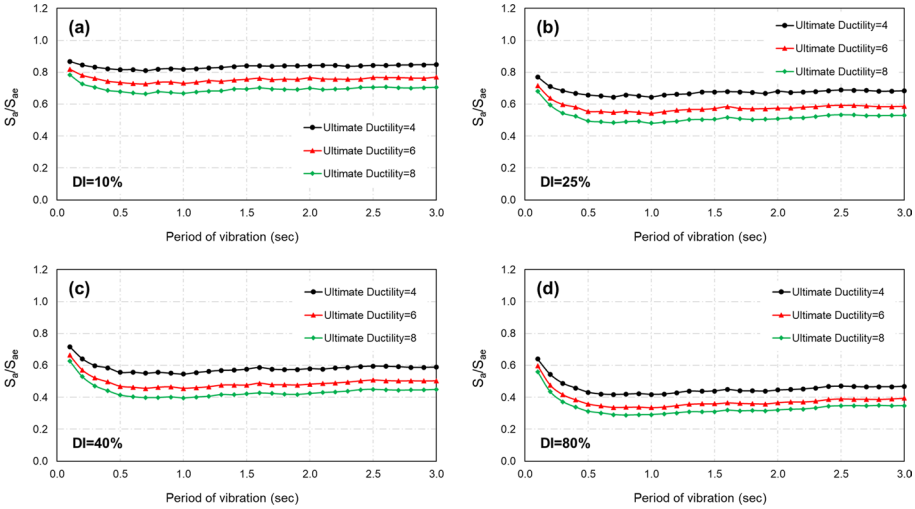

Fig. 5 The influence of ultimate ductility on damage-based response acceleration ratio

Table 5 Constant parameters based on nonlinear regression analysis for estimating damage-based response acceleration ratio

Ultimate ductility	DI	EPP		MC		MSD		SSD	
		a	b	a	b	a	b	a	b
$\mu_u = 4$	0.10	0.83	31.94	0.85	19.74	0.85	16.96	0.85	15.85
	0.25	0.67	61.00	0.67	40.69	0.67	39.08	0.67	32.87
	0.40	0.57	107.4	0.56	33.11	0.56	29.40	0.55	26.18
	0.80	0.44	301.3	0.41	89.85	0.41	76.48	0.41	59.35
$\mu_u = 6$	0.10	0.75	14.69	0.76	10.20	0.76	8.70	0.76	8.230
	0.25	0.57	40.97	0.56	27.71	0.56	25.50	0.56	20.82
	0.40	0.48	81.82	0.45	24.11	0.45	20.80	0.45	17.66
	0.80	0.36	252.1	0.32	82.54	0.32	64.57	0.33	52.14
$\mu_u = 8$	0.10	0.69	10.47	0.69	7.38	0.70	6.730	0.70	5.916
	0.25	0.51	34.30	0.49	22.84	0.49	20.68	0.49	16.36
	0.40	0.42	72.24	0.39	21.47	0.39	18.59	0.39	14.93
	0.80	0.32	243.1	0.28	78.86	0.28	62.84	0.28	52.10

nonlinear least-square regression analysis using the Levenberg–Marquardt method (Bates and Watts 1988) in Excel software. The presented constant parameters relate to damage level, ultimate ductility of the system, and the hysteresis model.

$$\frac{S_a}{S_{ae}} = a + b\left[\frac{DI}{T}\right]^2 \tag{3}$$

where T is the fundamental period of SDOF system, DI is the damage index, and a, b are constant parameters based on Table 5.

The bias and standard deviation of the proposed equation was obtained based on following equations, given as:

$$E_{T,DI} = \left[\frac{C_{Sa-i(app)}}{C_{Sa-i(ex)}}\right]_{DI} \tag{4}$$

$$\sigma_{T,DI} = \sqrt{\frac{1}{n-1}\sum_{i=1}^{n}\left[\left(E_{T,DI}\right) - \left(\overline{E}_{T,DI}\right)\right]^2} \tag{5}$$

$$\overline{E}_{T,DI} = \frac{1}{n}\sum_{i=1}^{n}\left(E_{T,DI}\right)_i \tag{6}$$

where $C_{Sa-i(app)}$ is the estimated response acceleration ratio, $C_{Sa-i(ex)}$ is the exact response acceleration ratio from the direct time history analysis, n is the number of data, $E_{T,DI}$ is the bias, and $\overline{E}_{T,DI}$ is the mean error.

It is worth mentioning that the bias and standard deviation of the proposed equation are presented to indicate the accuracy of the formula for estimating the damage-based acceleration response ratio. Values of $E_{T,DI}$ higher than one show an overestimation of the proposed equation, and lower than one illustrates an underestimation. Moreover, values of $\sigma_{T,DI}$ as lower than possible indicate a more robust estimation. Figures 6 and 7 demonstrate that the bias and standard deviation at different periods of vibration, damage level, and ultimate ductility of the system are not high and unacceptable. Figure 6 indicates that the bias increases by increasing the damage level and ultimate ductility of the system, which is predictable because the variation among data is amplified in higher values. The mentioned trend is correct in standard deviation among data, according to Fig. 7. Hence, the suggested equation can predict the response acceleration ratio with lower error.

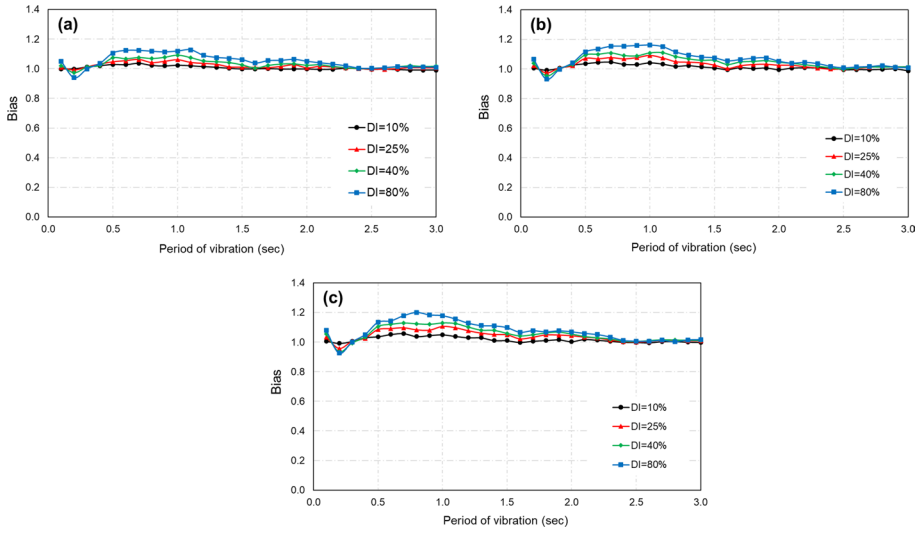

Fig. 6 The bias at **a** $\mu_u = 4$, **b** $\mu_u = 6$, **c** $\mu_u = 8$

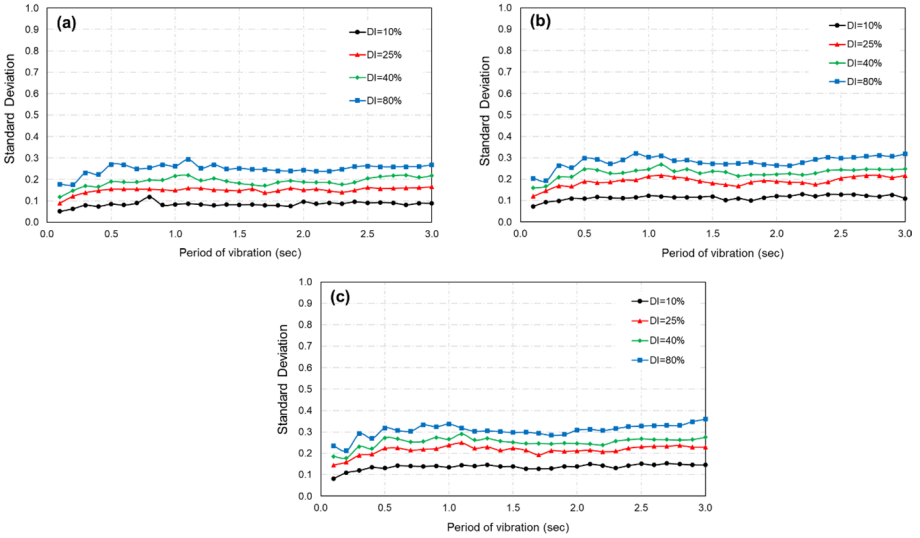

Fig. 7 The standard deviation at **a** $\mu_u = 4$, **b** $\mu_u = 6$, **c** $\mu_u = 8$

Step 4: In the fourth step, the damage-based strength reduction factor must be determined according to $R_{DI} = \frac{mS_a}{F_y} = \frac{F_e}{F_y}$, where m is the mass, F_e is the elastic strength of the SDOF system, and F_y is the yield strength of the system at desired damage level. Therefore, the strength reduction factor of the SODF system was utilized at 0.1 to 3 s period of vibration, four damage levels, and three ultimate ductility factors. Figure 8 shows the $DI - T - R_{DI}$ relation at different damage levels, periods, and ultimate ductility factors, where the R_{DI} increases by increasing damage levels. Based on the figure, the R_{DI} is sensitive in the short-period region, and mentioned sensitivity increases with the growth of

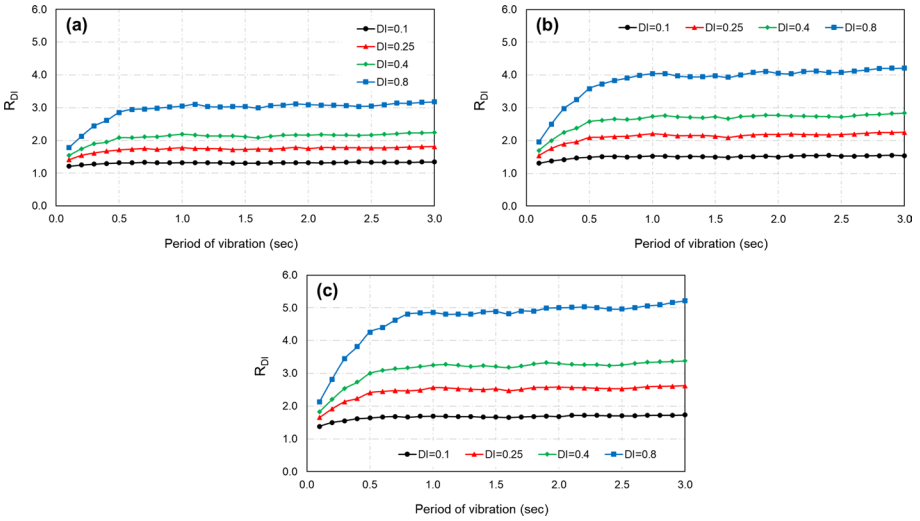

Fig. 8 The R-DI-T relationship at **a** $\mu_u = 4$, **b** $\mu_u = 6$, **c** $\mu_u = 8$

the damage level. Also, the R_{DI} becomes constant at medium period ranges, from 0.5 to about 1s, which is related to the level of damage and ultimate ductility. It is necessary to explain that the R_{DI} values are affected by the ultimate ductility of the system proportionally, where the R_{DI} illustrates higher values in higher ductility levels. The COV in the $DI - T - R_{DI}$ relation is below 0.35 and not too high, which is not presented due to space limitations in the paper.

According to observed data, a simplified equation based on the $DI - T - R_{DI}$ relation is suggested to evaluate R_{DI} in each period of vibration, damage level, and ultimate ductility using the nonlinear regression analysis (similar to Eq. 3), given as:

$$R_{DI} = a + [b \times DI] * exp^{(cT)} \tag{7}$$

where DI is the damage index, T is the period of vibration in SDOF system, and a, b, c are constant parameters achieved from nonlinear regression analysis, presented in Table 6.

Step 5: In the fifth step, the nonlinear pushover analysis must be performed by subjecting the structure to a monotonic lateral load pattern. The mentioned analysis would help to find internal forces when the structural system is subjected to earthquake ground shaking. The structural elements yield subsequently, and the stiffness loss occurred due to the increment of the lateral load pattern in the system. Then, the force–displacement relation would be determined by pushover analysis of the MDOF system (multi-degree-of-freedom). The total base shear and top roof displacement at the control node should be considered in the $F - \Delta$ relation, respectively. The appropriate lateral load pattern is a significant issue in pushing the structure to target displacement. In this investigation, the lateral load pattern was defined based on ASCE/SEI 41-17 recommendation, where the vector of lateral loads is specified as follows:

$$P = p\psi = pM\varphi \tag{8}$$

where M is the mass matrix, and φ is the displacement shape. The magnitude and distribution of lateral load are controlled by p and ψ. The lateral force in the i-th floor level is equivalent to φ_i of the assumed displacement shape φ, weighted by the story mass M_i, given as:

$$P_i = pM_i\varphi_i \tag{9}$$

Step 6: In the sixth step, the equivalent SDOF model and capacity diagram must be developed to construct the idealized force–displacement curve. The equation of motion for MDOF systems only consists of the lateral translational degree of freedom, given as:

$$M\ddot{U} + C\dot{U} + R = M1\ddot{u}_g \tag{10}$$

where M is the mass matrix, C is the damping matrix, 1 is the unit vector, $\ddot{u_g}$ is the ground motion acceleration, and U and R are displacements and internal force vectors, respectively. The displacement vector of the structural frame at a generic time is:

$$U = \Phi x_t \tag{11}$$

where $\{\Phi\}$ is displacement shape and x_t expresses the time-dependent top displacement of structure.

Based on static, $P = R$, where internal forces R are equal to external loads P. Therefore, Eq. (11) can be expressed as:

Table 6 Constant parameters based on nonlinear regression analysis for estimating R_{DI}

Ultimate ductility	DI	EPP			MC			MSD			SSD		
		a	b	c	a	b	c	a	b	c	a	b	c
$\mu_u = 4$	0.10	1.33	−1.84	−4.68	1.30	−1.64	−2.80	1.30	−1.82	−2.87	1.30	−1.91	−2.84
	0.25	1.77	−2.22	−4.41	1.76	−2.38	−3.13	1.76	−2.46	−3.06	1.76	−2.73	−3.23
	0.40	2.17	−2.34	−4.00	2.22	−2.65	−2.98	2.22	−2.77	−2.98	2.22	−3.18	−3.24
	0.80	3.09	−2.41	−3.71	3.33	−2.88	−2.81	3.34	−3.14	−2.87	3.35	−3.47	−2.86
$\mu_u = 6$	0.10	1.52	−3.30	−4.32	1.49	−3.34	−3.10	1.49	−3.72	−3.24	1.48	−3.83	−3.18
	0.25	2.18	−3.83	−3.99	2.23	−4.28	−2.95	2.23	−4.49	−2.93	2.23	−5.08	−3.16
	0.40	2.76	−3.87	−3.72	2.92	−4.50	−2.75	2.92	−4.88	−2.81	2.93	−5.43	−2.90
	0.80	4.09	−3.76	−3.32	4.59	−4.68	−2.66	4.65	−5.10	−2.60	4.63	−5.16	−2.32
$\mu_u = 8$	0.10	1.70	−4.85	−4.23	1.68	−5.06	−3.01	1.68	−5.35	−3.05	1.67	−5.82	−3.21
	0.25	2.55	−5.32	−3.79	2.67	−6.12	−2.78	2.67	−6.51	−2.79	2.68	−7.45	−3.05
	0.40	3.29	−5.28	−3.53	3.56	−6.34	−2.71	3.58	−6.94	−2.77	3.59	−7.44	−2.69
	0.80	5.00	−4.95	−3.11	5.79	−6.41	−2.51	5.86	−6.94	−2.40	5.81	−6.98	−2.26

$$\Phi^T M\Phi\ddot{x}_t + \Phi^T C\Phi\dot{x}_t + \Phi^T M\Phi p = -\Phi^T M1\ddot{u}_g \tag{12}$$

The equation of motion for the equivalent SDOF system is determined by dividing the left hand in Eq. (12) to $-\Phi^T M1$, given as:

$$m^*\ddot{x} + F^* = -m^*\ddot{u}_g \tag{13}$$

where the m^*, F^*, and D^*, known as equivalent mass, force, and displacement of the equivalent SDOF system, is given by:

$$m^* = \Phi^T M1 = \sum m_i\Phi_i \tag{14}$$

$$D^* = \frac{x_t}{\Gamma} \tag{15}$$

$$F^* = \frac{V}{\Gamma} \tag{16}$$

where V is base shear in MDOF system, expressed as:

$$V = \sum P_i = \Phi^T M1p = p\sum m_i\Phi_i = pm^* \tag{17}$$

The Γ parameter controls the transformation from MDOF to the SDOF model, which is called as modal participation factor. The Γ is:

$$\Gamma = \frac{\Phi^T M1}{\Phi^T M\Phi} = \frac{\sum m_i\Phi_i}{\sum m_i{\Phi_i}^2} = \frac{m^*}{\sum m_i{\Phi_i}^2} \tag{18}$$

It is worth mentioning that the Γ is equal to PF_1 in the capacity spectrum method and C_1 in the coefficient method based on ATC-40 (1996) and ASCE/SEI 41-17 codes (ASCE/SEI 41-17 2017), respectively. Hence, the bilinear Force–Displacement curve for the equivalent SDOF can be determined using the equal energy method where the area under pushover and the idealized bilinear curve are the same. The elastic period of vibration in the idealized bilinear curve is specified as follows:

$$T^* = 2\pi\sqrt{\frac{m^*D_y^*}{F_y^*}} \tag{19}$$

where D_y^* and F_y^* are yield displacement and strength of the system, respectively.

In the end, the idealized bilinear Force–Displacement diagram must be converted to the S_a-Displacement diagram, known as ADRS format, according to the following equation:

$$S_a = \frac{F^*}{m^*} \tag{20}$$

Step 7: In the seventh step, the seismic demand for the SDOF model must be determined regarding Eqs. (21) to (22) proposed by Fajfar (1999, 2000). It should be noted that the R in Eq. (21) is damage-based, which leads to the estimation of S_d in the desired damage level.

$$R_{DI} = \frac{S_{ae}}{S_{ay}} \tag{21}$$

$$\left\{ \begin{array}{c} S_d = \frac{S_{de}}{R_{DI}}\left(1 + \left(R_{DI} - 1\right)\frac{T_C}{T^*}\right) if T^* < T_c \\ S_d = S_{de} if T^* \geq T_c \end{array} \right\} \tag{22}$$

where S_{ae} is the elastic response acceleration, S_{ay} is the yield response acceleration, S_{de} is the elastic spectral displacement, T_C is the characteristic period of vibration related to the demand curve, T^* is the elastic period, R_{DI} is the strength reduction factor related to damage, and S_d is the target displacement.

The seismic demand and capacity in ADRS format are plotted in Fig. 9 to represent structures with $T^* < T_c$ and $T^* \geq T_c$ conditions, respectively. Based on the figure, the intersection of the dotted line corresponds to the elastic period in the idealized capacity curve with elastic demand in ADRS format is S_{ae}, known as elastic response acceleration and elastic displacement. In both conditions of $T^* < T_c$ and $T^* \geq T_c$, the intersection of capacity and inelastic demand correspond to the desired damage level.

3 Experimental models for verification

In this paper, two experimental reinforced concrete (RC) bridge pier systems were numerically modeled to verify the proposed method with the fiber element models (FEM) for better understanding. Schoettler et al. (2015) presented a comprehensive report about the RC bridge pier under uniaxial shake table analysis under sequential earthquake ground motions with required time gaps between them. The mentioned time gap was used between earthquake records to cease the system after excitation (Abdollahzadeh et al. 2023). The ground motions were selected from low to high intensity to bring the system near collapse condition, reference to Table 7. It is worth mentioning that the RC bridge pier was designed according to Caltrans provision (Caltrans 2010) and tested at the University of California (Berkeley), as shown in Fig. 10. The model characteristics are presented in Table 8, including material properties and section dimensions.

The RC bridge pier with hollow section configuration was selected in this investigation as a second empirical model, tested by Petrini et al. (2008) in Pavia (Italy) under dynamic analysis. As indicated in Fig. 11, the RC bridge pier was constructed in two sections,

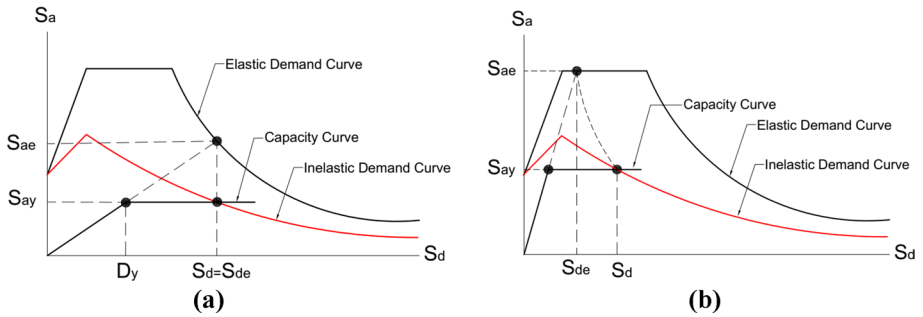

Fig. 9 Estimation of target displacement for structures with **a** $T^* < T_c$ and **b** $T^* \geq T_c$ conditions

Table 7 Ground motion characteristics used in verification (Schoettler et al. 2015)

Test	Earthquake	Date	Mw	Station	Comp	Scale factor	PGA (g)	PGV (m/s)
EQ1	Loma Prieta	10/18/1989	6.9	Agnew State Hospital	90	1	− 0.199	0.16
EQ2	Loma Prieta	10/18/1989	6.9	Corralitos	90	1	0.409	0.37
EQ3	Loma Prieta	10/18/1989	6.9	LGPC	0	1	0.526	0.89
EQ4	Loma Prieta	10/18/1989	6.9	Corralitos	90	1	0.454	0.39
EQ5	Kobe	1/16/1995	6.9	Takatori	0	− 0.8	− 0.533	0.95
EQ6	Loma Prieta	10/18/1989	6.9	LGPC	0	1	− 0.512	0.87

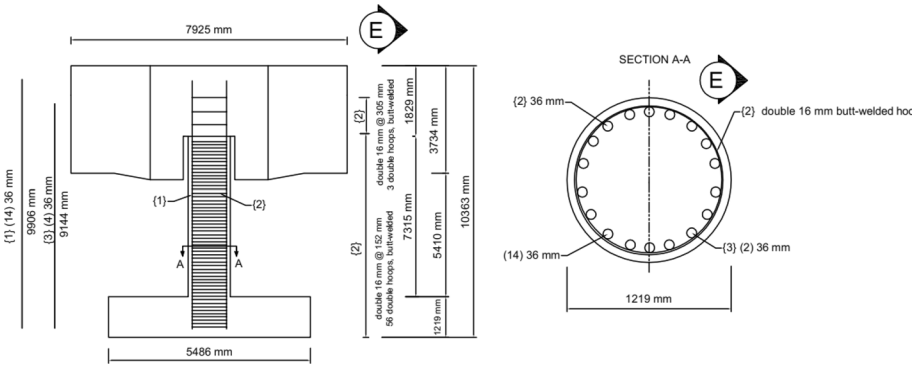

Fig. 10 Full-scale RC bridge pier specimen and cross-section (Schoettler et al. 2015)

Table 8 Material properties and pier dimensions (Schoettler et al. 2015; Amirchoupani et al. 2021)

Parameters	Values	Remarks
Column diameters (m)	1.22	–
Column height (m)	7.32	–
Concrete cover (mm)	50	–
Longitudinal reinforcement diameter (mm)	18 Φ 35.8	ρ = 1.55%
Yield stress (MPa)	519	–
Ultimate stress (MPa)	707	–
Initial elastic tangent (MPa)	196,000	–
Tangent at initial strain hardening (MPa)	5520	–
Strain corresponding to initial strain hardening (%)	1.1	–
Strain at peak stress (%)	12.2	–
Transverse reinforcement diameter (mm)	15.9 @ 152	ρ = 0.95%
Yield stress (MPa)	338	–
Ultimate stress (MPa)	592	–
Strain at peak stress (%)	12.5	–
Axial load (MN)	2.32	–

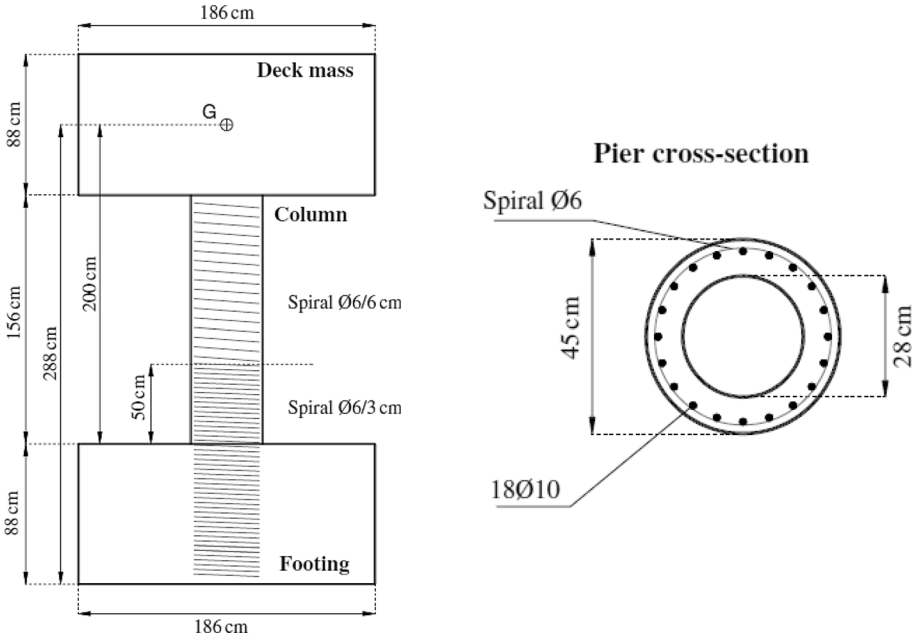

Fig. 11 Configuration of hollow section bridge pier specimen (Petrini et al. 2008)

including eighteen longitudinal bars confined with 30-millimeter transversal spiral pitches from a 50-centimeter distance from the foundation and 60-millimeter spiral pitches in the upper parts. Table 9 presents the pier dimensions and material properties used in the empirical model. It should be noted that the simulation of ground shaking was performed under the Morgan Hill event in 1984 with $M_w = 6.2$ and PGA = 0.15 g using shake table analysis.

The fiber-based modeling was adapted using the 3D nonlinear beam-column element with five integration points along height by Open System for Earthquake Engineering Simulation (OpenSEES) software (Mazzoni et al. 2006) for numerically modeling the empirical cited

Table 9 Dimensions and material properties in Petrini et al. (2008) model (Amirchoupani et al. 2021)

Parameters	Values	Remarks
Column diameters (m)	0.45	–
Column height (m)	2	–
Concrete cover (mm)	25	–
Longitudinal reinforcement diameter (mm)	18 Φ 10	–
Yield stress (MPa)	514	–
Ultimate stress (MPa)	707	–
Initial elastic tangent (MPa)	210,000	–
Transverse reinforcement diameter (mm)	Φ6 @ 30	ρ = 0.93%
Yield stress (MPa)	514	–
Ultimate stress (MPa)	707	–
Axial load (KN)	78	–

models. The Concrete02 material based on Kent and Park's (1971) hysteresis model was used to model the unconfined (cover) and confined (core) part of the section, and reinforcing material based on the Coffin-Manson equation was defined to consider the mechanical effect of compressive buckling, the transition from elastic behavior to inelastic, strain softening, and low-cycle fatigue, regarding OpenSEES library (the $\alpha=0.506$, $C_f=0.361$, $C_d=0.6$ was used in Coffin-Manson model).

The pier section in different integration points was divided into 150 mesh elements to attain accurate results (Fig. 12a). Moreover, the bond-slip behavior was considered to model the member end rotation regarding the strain penetration between the foundation and RC pier. Hence, the mentioned procedure was employed by defining a zero-length section to compute moment–curvature responses according to bond-slip behavior, as illustrated in Fig. 12b to c. The pointed method (bond-slip modeling with zero-length section) was employed by Zhao and Sritharan (2007), utilizing six parameters to capture bond-slip influence in the connection between elements, as indicated in Fig. 12c.

The S_y and S_u were computed by Eqs. (23) and (24), given as:

$$S_y = 2.54\left[\frac{d_b}{8437}\frac{F_y}{\sqrt{f_c}}(2\alpha+1)\right]^{1/\alpha} + 0.34 \tag{23}$$

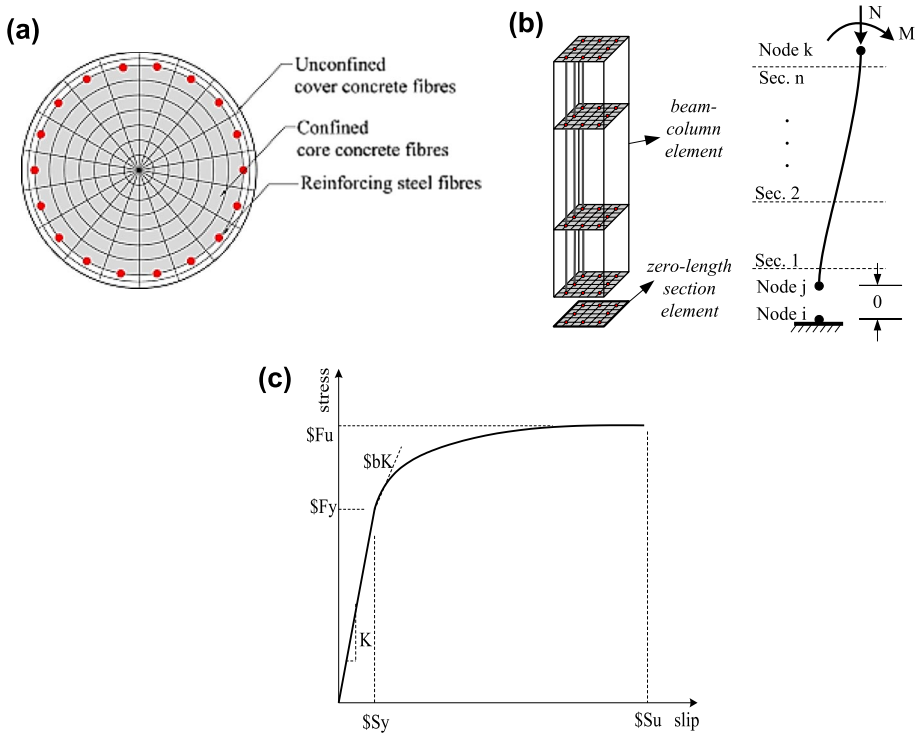

Fig. 12 **a** Fiber section model **b** Distribution of plastic hinge with bond-slip behavior **c** Uniaxial bond-slip material (Zhao and Sritharan 2007)

$$S_u = 30 \sim 40 S_y \tag{24}$$

where d_b is rebar diameter in mm units, F_y is yield strength (MPa), f_c is the compressive strength of concrete material, α is the constant parameter taken as 0.4 based on CEB-FIP model code 90, and b is initial hardening ratio in the monotonic slip versus bar responses (the $S_y = 0.548$, $S_u = 19.18$, $b = 0.4$, $R = 0.75$ parameters were used in Schoettler et al. (2015) model and $S_y = 0.35$, $S_u = 12.21$, $b = 0.4$, $R = 0.75$ for Petrini et al. (2008) model).

The appropriate verification between the empirical and numerical model of Schoettler et al. (2015) under six sequentially ground motions, based on Table 7, is illustrated in Fig. 13. Moreover, the accuracy of Petrini et al. (2008) model under dynamic analysis is presented in Fig. 14. It is worth mentioning that some inaccurate responses between empirical and numerical models arise from solver algorithms and uncertainties in the construction of the empirical model.

4 Designed models for verification

In this investigation, three 1-, 7-, and 10-story steel moment resistance structural systems were designed based on ASCE/SEI 7-16 (ASCE/SEI 7-16 2016) loading requirements and AISC 360-16 (AISC 360-16 2016) design requirements to validate the proposed method in different period ranges. The ordinary moment resisting system (OMF) was considered for 1-story, and the intermediate frame (IMF) for 7- and 10-story structures. The response modification factor (R), deflection amplification factor (Cd), and system overstrength (Ω)

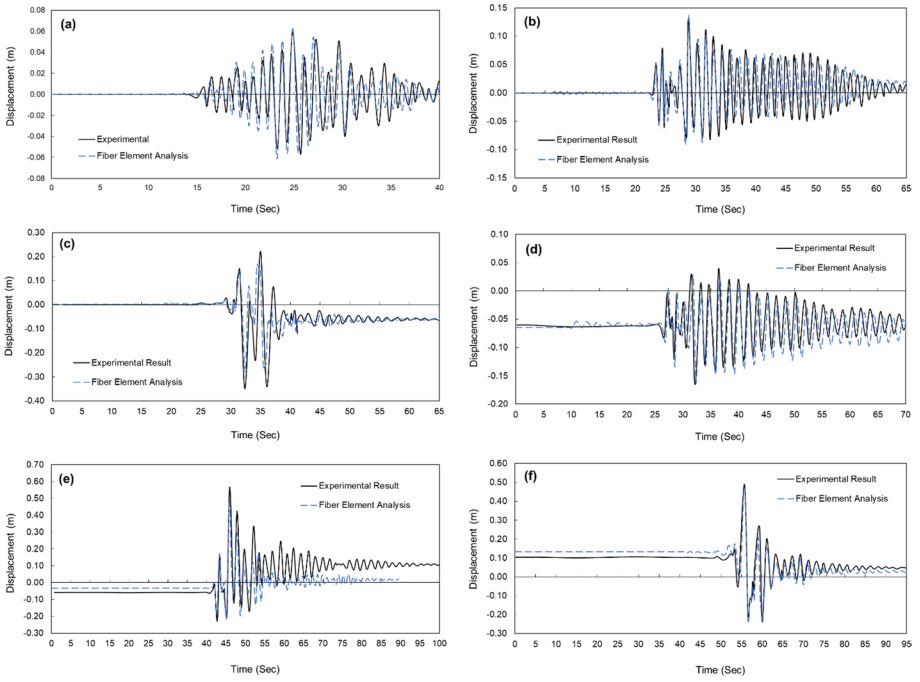

Fig. 13 Verification between empirical shake table analysis and numerical fiber-based model

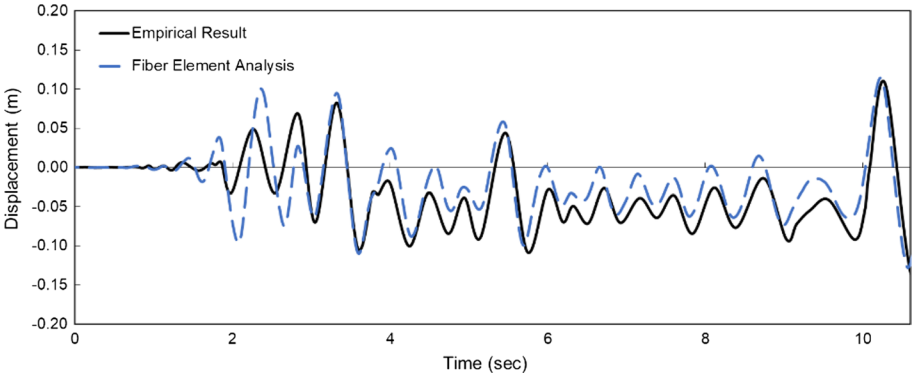

Fig. 14 Verification between empirical Petrini et al. (2008) model and numerical fiber-based model

for the 1-story structure was defined as 3.5, 3, 3, and 8, 5.5, 3 for 7- and 10-story. The 3000 kg/cm^2 dead load and 1000 kg/cm^2 live load were considered with seismic load under design seismic hazard level (DE), where the spectral acceleration in short- and long-periods was 0.842 g and 0.379 g, respectively. Moreover, the 5m span length and 3.5 m height are constant in all models, where the total height of 1-, 7-, and 10-story structures are 3.5 m, 24.5 m, and 35 m, respectively. The drift value under seismic load (linear design) is lower than 2.5% for 1-story and 2% for 7- and 10-story. Figure 15 shows the configuration

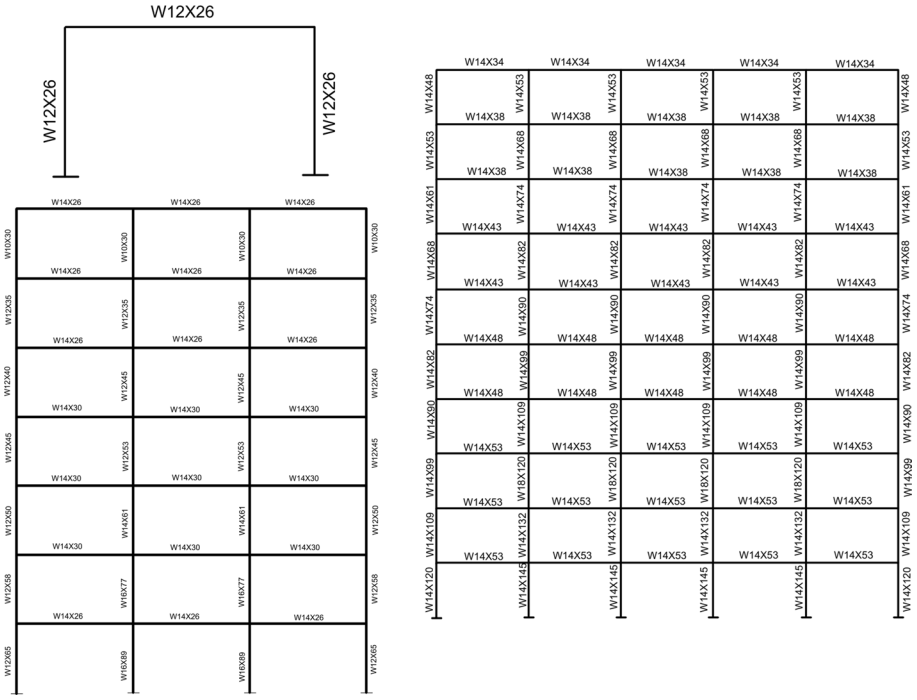

Fig. 15 The configuration of designed 1-story, 7-story, and 10-story models

of designed models and their section properties (W-shape) designed using steel material with 2400 kg/cm^2 yield stress and 3700 kg/cm^2 ultimate stress.

5 Discussion

In the first step, the eigenvalue analysis was performed to determine the period of vibration with a higher than 90% mass participating ratio, which it used in the scaling of ground motions from 0.2T to 1.5T for dynamic time history analysis and determination of R_{DI} in Eq. (7) and S_d in Eq. (22). Table 10 shows the three first periods of structural systems, including two empirical bridge piers and three steel moment structures. In the second step, the pushover analysis on two empirical and three designed models was performed up to the collapse condition. Then, the idealized pushover curve was determined by transforming the MDOF system to an equivalent SDOF system in the base-shear vs top-displacement plot. Figure 16 illustrates the pushover curves of selected models under nonlinear static analysis and the idealized curve up to the collapse condition. The structural properties, including effective stiffness, structural mass, yield strength, yield displacement, and ultimate ductility, are presented in Table 11.

As explained before, four hysteresis models were considered in this investigation to obtain the target displacement and performance point regarding the probable future earthquakes. Therefore, the cyclic displacement analysis, known as quasi-static analysis, was performed under the SAC loading protocol to obtain the hysteresis behavior of the considered models. Figure 17 illustrates the hysteresis behavior of the two verified empirical bridge piers and two 1- and 7-story steel moment structures, respectively. As indicated in Fig. 17, the hysteresis behavior of RC bridge piers and steel moment structures is similar to MD and EPP hysteresis models, respectively. It is worth mentioning that the cyclic displacement analysis of the 10-story model has not represented due to the identical behavior of this model to 1- and 7-story models. Therefore, the MD and EPP hysteresis behaviors were considered to calculate the constant parameters in obtained equations for estimating the target displacement of RC bridge piers and steel moment structures as the third step.

In the fourth step, sixteen earthquake records from Table 2 with appropriate spectral matching with seismic hazard level were selected to verify the applicability of the proposed method. Table 12 presents the ground motion characteristics from the PEER NGA West-2 project. It is necessary to explain that the chosen ground motions are based on $S_{DS} = 0.842$g and $S_{D1} = 0.3795$g hazard level. In the fifth step, the nonlinear displacement of the top story and structural damage index were determined under $S_{DS} = 1.684$g and $S_{D1} = 0.759$g seismic level. The cited seismic hazard level was considered to evaluate selected structures for putting them in higher nonlinearity conditions because higher nonlinearity is generally accompanied by the growth of

Table 10 Fundamental period of vibration in empirical and designed models

Modes	Schoettler et al. bridge pier	Petrini et al. bridge pier	1-story	7-story	12-story
First mode	0.616	0.169	0.335	1.938	3.064
Second mode	0.571	0.031	0.034	0.668	1.037
Third mode	–	–	0.034	0.378	0.607

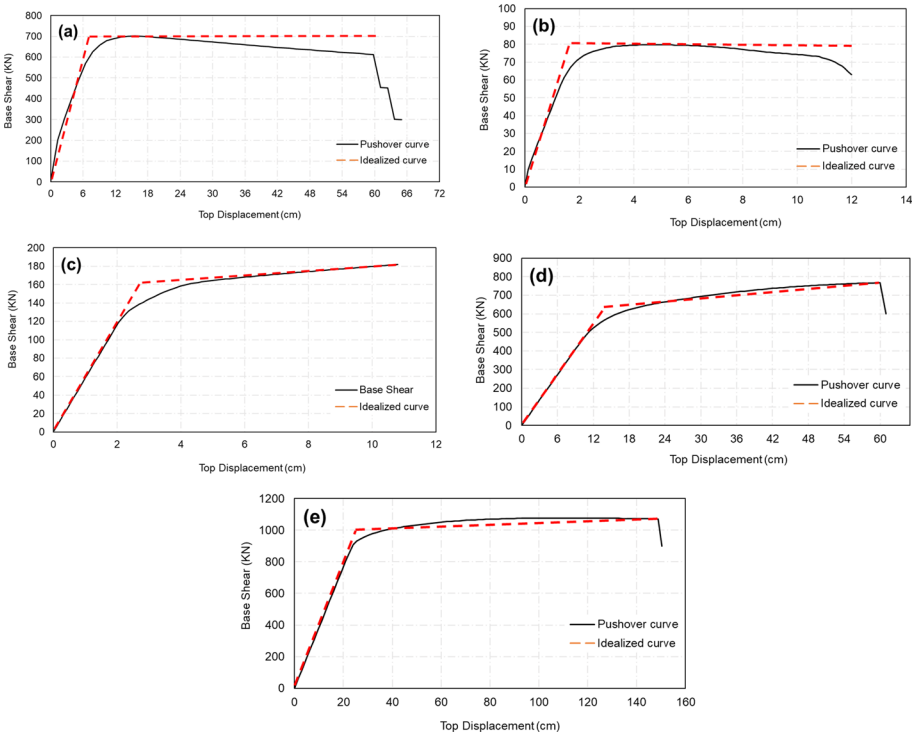

Fig. 16 The pushover analysis of selected models, including **a** Schoettler et al. (2015) bridge pier **b** Petrini et al. (2008) bridge pier **c** 1-story **d** 7-story **e** 10-story

Table 11 Structural characteristics under pushover analysis

Models	F_y (KN)	D_y (cm)	Mass (kg)	Effective stiffness (N/m)	Ultimate ductility
Schoettler et al. bridge pier	700	7.5	228,000	9,333,333.3	8
Petrini et al. bridge pier	80	1.8	7800	4,444,444	6.7
1-story	160	2.7	16,709	5,825,056	4
7-story	600	12.5	352,854	4,666,666	4.5
10-story	1000	26	841,946	3,846,153	5.8

dispersion and a decrease in the estimation accuracy. In the sixth step, the selected ground motions were scaled to the desired seismic hazard level. Although different ground motion scaling methodologies exist (Kurama and Farrow 2003; Naeim et al. 2004; ASCE/SEI 7-10 2010; Weng et al. 2010; Kalkan and Chopra 2011; O'Donnell et al. 2013; ASCE/SEI 7-16 2016), the normalizing-scaling theory proposed by Amirchoupani et al. (2020) was used to reduce the dispersion among acceleration responses, displacements, and damage index values. In this method, the spectral response acceleration of each record in the acceleration- (if $0.05s < T < 0.5s$), velocity- (if $0.5s < T < 2.7s$), and displacement-sensitive regions (if $2.7s < T < 4s$) were normalized

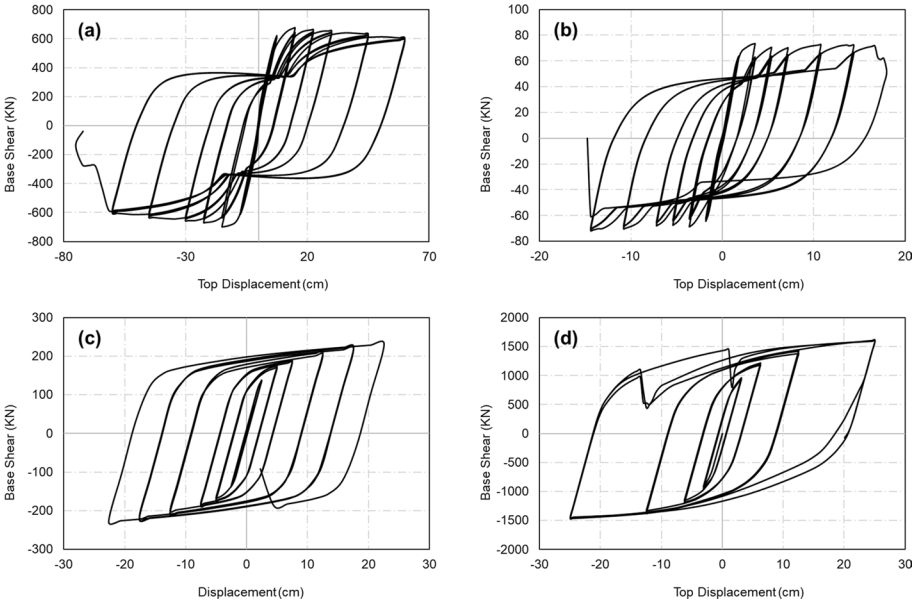

Fig. 17 The cyclic displacement analysis of selected models, including **a** Schoettler et al. (2015) bridge pier **b** Petrini et al. (2008) bridge pier **c** 1-story **d** 7-story

to their acceleration spectrum intensity, Housner intensity, and peak ground displacement, as a first level. The pointed parameters reach one by normalizing response accelerations to the normalizing index. Then, the scaling procedure based on ASCE/SEI 7 code would be performed as a next step.

In the seventh step, the mean top displacement and general damage index were obtained under dynamic time history analysis, according to ground motions in Table 12. Ghosh et al. (2011) concluded that the Park-Ang damage model could determine based on two global and local approaches to evaluate structural performance. Based on the global approach, the Park-Ang damage index is equal to Eq. (1), but the Park-Ang damage index is $DI = (x_{mi} - x_{yi})/(x_{ui} - x_{yi})|_{max} + \beta/V_y x_u \int dE_h$, based on the local approach where x_{mi} is the maximum drift in the i-th story level, x_{yi} is the yield value corresponding to the i-th inter-story ratio, and x_{ui} is the ductility capacity equals $\mu\ x_{ui}$. The damage index values in Table 13 were determined using the global Park-Ang damage approach.

The transformation factor (Γ) cited in this study and N_2 theory is equal to PF_1 in ATC-40 (1996) and C_0 in the FEMA series (FEMA 356 2000). The transformation from SDOF to MDOF in Schoettlet et al. (2015), Petrini et al. (2008), and 1-story steel moment resisting frame structures are equal to 1, and in two 7- and 10-story steel structures are 1.44 and 1.5, respectively. Table 14 shows the compression of target displacement based on the approximated method in this study, known as DN_2, and Zhai et al. (2013b) approximate procedure regarding the coefficient method, corresponding to calculated damage values. As represented in Table 14, the target displacement with precise accuracy in structures with short-period duration is estimated compared to the coefficient method proposed by Zhai et al. (2013a, b). Unlike the short-period region, there is no significant difference between the two methods in the high-period structures.

Table 12 The ground motion characteristics used in verification

NO	RSN	Earthquake Name	Year	Station Name	M_W	Mechanism	Rjb (km)	Vs30 (m/sec)	Comp	PGA (cm/s)
1	57	San Fernando	1971	Castaic-Old Ridge Route	6.6	Reverse	19.33	450	21	314.3
2	125	Friuli (Italy)	1976	Tolmezzo	6.5	Reverse	14.97	505	0	350.3
3	139	Tabas_ Iran	1978	Dayhook	7.3	Reverse	0	471	L1	317.7
4	231	Mammoth Lakes	1980	Long Valley Dam	6.0	Normal oblique	12.56	537	0	422.1
5	250	Mammoth Lakes	1980	Long Valley Dam	5.9	Strike slip	9.65	537	0	927.3
6	265	Victoria_ Mexico	1980	Cerro Prieto	6.3	Strike slip	13.8	471	45	633.1
7	564	Kalamata (Greece)	1986	Kalamata (bsmt)	6.2	Normal	6.45	382	NS	234.0
8	589	Whittier Narrows	1987	Alhambra-Fremont School	5.9	Reverse oblique	1.67	549	180	284.1
9	690	Whittier Narrows	1987	San Gabriel-E Grand Ave	5.9	Reverse oblique	0	401	180	257.3
10	755	Loma Prieta	1989	Coyote Lake Dam	6.9	Reverse oblique	19.97	561	195	148.9
11	787	Loma Prieta	1989	Palo Alto-SLAC Lab	6.9	Reverse oblique	30.62	425	270	191.0
12	801	Loma Prieta	1989	San Jose-Santa Teresa Hills	6.9	Reverse oblique	14.18	671	225	271.1
13	1012	Northridge	1994	LA 00	6.6	Reverse	9.87	706	180	257.9
14	1512	Chi-Chi (Taiwan)	1999	TCU078	7.6	Reverse oblique	0	443	E	438.8
15	1787	Hector Mine	1999	Hector	7.1	Strike slip	10.35	726	0	260.4
16	2628	Chi-Chi (Taiwan)	1999	TCU078	6.2	Reverse	0	443	E	439.0

Table 13 Top displacement and global damage index obtained from time history analysis

NO	RSN	Schottler et al. Model		Petrini et al. Model		1-Story SMF		7-Story SMF		10-Story SMF	
		DI	D_{max}	DI	D_{max}	DI	D_{max}	DI	D_{max}	DI	D_{max}
1	57	0.24	0.119	0.12	0.024	0.52	0.052	0.28	0.239	0.21	0.489
2	125	0.23	0.16	0.13	0.025	0.41	0.05	0.18	0.218	0.22	0.449
3	139	0.30	0.165	0.06	0.019	0.41	0.047	0.34	0.302	0.31	0.535
4	231	0.27	0.159	0.06	0.018	0.50	0.053	0.31	0.243	0.30	0.626
5	250	0.20	0.12	0.08	0.024	0.32	0.047	0.08	0.13	0.05	0.283
6	265	0.28	0.145	0.10	0.024	0.55	0.06	0.17	0.212	0.30	0.612
9	564	0.18	0.129	0.14	0.026	0.48	0.052	0.26	0.243	0.35	0.478
10	589	0.22	0.13	0.11	0.025	0.20	0.038	0.16	0.201	0.31	0.491
11	690	0.18	0.123	0.03	0.018	0.30	0.04	0.33	0.232	0.39	0.433
12	755	0.27	0.129	0.10	0.021	0.52	0.047	0.51	0.349	0.31	0.5
13	787	0.29	0.177	0.23	0.033	1.02	0.094	0.59	0.387	0.44	0.583
14	801	0.26	0.145	0.07	0.020	0.26	0.041	0.30	0.256	0.58	0.854
15	1012	0.20	0.137	0.21	0.031	0.59	0.058	0.15	0.196	0.39	0.608
16	1512	0.33	0.137	0.17	0.023	0.45	0.045	0.33	0.245	0.38	0.437
18	1787	0.42	0.199	0.14	0.023	0.36	0.043	0.24	0.231	0.33	0.479
20	2628	0.12	0.197	0.24	0.035	0.09	0.063	0.41	0.331	0.65	1.029
Mean		*0.25*	*0.148*	*0.15*	*0.024*	*0.4*	*0.049*	*0.30*	*0.251*	*0.35*	*0.555*

Table 14 Comparison between direct nonlinear displacement from time history analysis, and approximate DN_2, and Zhai et al. (2013b) method

Earthquake name	Scottler et al. model	Petrini et al. model	1-Story Steel moment frame	7-Story steel moment frame	10-story steel Moment Frame
Damage	0.250	0.150	0.400	0.300	0.350
This study	0.175	0.027	0.050	0.269	0.595
Zhai et al. (2013b)	0.116	0.019	0.043	0.271	0.599
Direct analysis	0.148	0.024	0.049	0.251	0.555
This study error	**18.094**	**9.179**	**1.902**	**7.211**	**7.082**
Zhai et al. (2013b) Error	*21.516*	*23.847*	*13.256*	*7.919*	*7.810*

Therefore, the target displacement in the long-period region is appropriately predicted in both methods. Hence, the target displacement can be obtained with acceptable accuracy due to the DN_2 method for structural systems in short- and long-period regions.

6 Conclusion

In this investigation, the N_2 theory based on the Park-Ang damage index model, called the damage-based N_2 method (DN_2), was developed to evaluate the target displacement and performance point in structural systems under far-field earthquake ground motions. Hence, the following procedure was recommended:

1. The damage-based response acceleration ratio for four hysteresis models, including EPP, MC, MSD, and SSD, were determined at four damage levels, four ultimate ductility factors, and 30 periods of vibration to predict the inelastic values from elastic ones. Then, a simplified equation was proposed to construct inelastic response accelerations regarding nonlinear regression analysis.
2. The damage-based strength reduction factor by the relation between the R_{DI}-T-DI was developed at four damage levels, four ultimate ductility factors, and 30 periods of vibration to estimate the structural damage at the desired hazard level. Then, a simplified equation was suggested to predict this value according to nonlinear regression analysis.
3. The inelastic displacement equations for structures with $T^* < T_c$ and $T^* \geq T_c$ conditions, recommended by Fajfar (2000), were used to estimate performance points and structural status.

The accuracy and applicability of the proposed method were investigated using two verified experimental reinforced concrete bridge piers and three steel moment-resisting frame structures. The mentioned models were subjected to sixteen earthquake ground motion records scaled to arbitrary seismic hazard levels higher than the design level to bring the models into highly nonlinear conditions. Then, the obtained nonlinear top displacements and damage index from direct time history analyses were compared with the DN_2 and damage-based coefficient methodologies suggested before. Statistical results show that:

1. The target displacement in short-period structures was appropriately evaluated by the DN_2 method compared to the coefficient method.
2. The target displacement in long-period structures with a duration higher than 1s was appropriately assessed by both the DN_2 and coefficient methods.
3. The error between obtained top displacements under direct history analysis and DN_2 approximate procedure was below 10% (except in full-scale bridge pier), while the coefficient method shows higher error values.

Funding The authors have not disclosed any funding.

Declarations

Conflict of interest The authors declare that no funds, grants, or other support were received during the preparation of this manuscript.

References

Abdollahzadeh G, Pourkalhor S, Vakhideh A, Pourbahram Z, Amirchoupani P (2023) Quantifying the optimal time gap between consecutive events. Asian J Civ Eng 24:1373–1392. https://doi.org/10.1007/s42107-023-00575-8

AISC 360–16 (2016) Specification for structural steel buildings, American Institute of Steel Construction, Chicago, IL, USA

Amirchoupani P, Abdollahzadeh G, Hamidi H (2020) Spectral acceleration matching procedure with respect to normalization approach. Bull Earthq Eng 18:5165–5191. https://doi.org/10.1007/s10518-020-00897-x

Amirchoupani P, Abdollahzadeh G, Hamidi H (2021) Improvement of energy damage index bounds for circular reinforced concrete bridge piers under dynamic analysis. Struct Concr 22:3315–3335. https://doi.org/10.1002/suco.202000762

Amirchoupani P, Farahani RN, Abdollahzadeh G (2023a) The constant damage inelastic displacement ratio for performance design of self-centering systems under far-field earthquake ground motions. Structures 57:105254. https://doi.org/10.1016/j.istruc.2023.105254

Amirchoupani P, Abdollahzadeh G, Hamidi H (2023b) Development of inelastic displacement ratio using constant energy-based damage index for performance-based design. Bull Earthq Eng 21:3461–3491. https://doi.org/10.1007/s10518-023-01652-8

ASCE/SEI 41-17 (2017) Seismic evaluation and retrofit of existing buildings, American Society of Civil Engineers, Washington, DC, USA. https://doi.org/10.1061/9780784414859

ASCE/SEI 7-10 (2010) Minimum Design Loads for Buildings and Other Structures. American Society of Civil Engineers, Reston, VA, USA

ASCE/SEI 7-16 (2016) Minimum Design Loads and Associated Criteria for Buildings and Other Structures. American Society of Civil Engineers, Reston, VA, USA

ATC-40 (1996) Seismic analysis and retrofit of concrete buildings. Applied Technology Council, Redwood City, CA, USA

Baez JI, Miranda E (2000) Amplification factors to estimate inelastic displacement demands for the design of structures in the near field. Proceedings of 12th World Conference on Earthquake Engineering

Bates DM, Watts DG (1988) Nonlinear regression analysis and its applications. Wiley, New York

Bhatt C, Bento R (2011) Assessing the seismic response of existing RC buildings using the extended N2 method. Bull Earthq Eng 9:1183–1201

Boore DM, Joyner WB, Fumal TE (1997) Equations for estimating horizontal response spectra and peak acceleration from western North American earthquakes: a summary of recent work. Seismol Res Lett 68:128–153. https://doi.org/10.1785/gssrl.68.1.128

Caltrans SDC (2010) Caltrans seismic design criteria version 1.6. California Department of Transportation, Sacramento, CA, USA

Decanini LD, Bruno S, Mollaioli F (2004) Role of damage functions in evaluation of response modification factors. J Struct Eng 130:1298–1308

Diaz SA, Pujades LG, Barbat AH et al (2017) Energy damage index based on capacity and response spectra. Eng Struct 152:424–436. https://doi.org/10.1016/j.engstruct.2017.09.019

Dolšek M, Fajfar P (2007) Simplified probabilistic seismic performance assessment of plan-asymmetric buildings. Earthq Eng Struct Dyn 36:2021–2041

Fajfar P (1999) Capacity spectrum method based on inelastic demand spectra. Earthq Eng Struct Dyn 28:979–993

Fajfar P (2000) A nonlinear analysis method for performance-based seismic design. Earthq Spectra 16:573–592

Fajfar P, Gašperšič P (1996) The N2 method for the seismic damage analysis of RC buildings. Earthq Eng Struct Dyn 25:31–46

Fajfar P, Fischinger M (1988) N2-A method for non-linear seismic analysis of regular buildings. In: Proceedings of the ninth world conference in earthquake engineering, Tokyo, Japan

Farahani RN, Abdollahzadeh G, Roshan AMG (2023) The modified energy-based method for seismic evaluation of structural systems with different hardening ratios and deterioration hysteresis models. Periodica Polytechnica Civil Eng. https://doi.org/10.3311/PPci.21359

FEMA-273 (1997) Commentary on the guidelines for seismic rehabilitation of buildings. Federal Emergency Management Agency, Washington, DC, USA

FEMA-356 (2000) Prestandard and commentary for the seismic rehabilitation of buildings. Federal Emergency Management Agency, Washington, DC, USA

FEMA-440 (2005) Improvement of Nonlinear Static Seismic Analysis Procedures. Federal Emergency Management Agency, Washington, DC, USA

Ghobarah A, Abou-Elfath H, Biddah A (1999) Response-based damage assessment of structures. Earthq Eng Struct Dyn 28:79–104. https://doi.org/10.1002/(SICI)1096-9845(199901)28:1%3c79::AID-EQE805%3e3.0.CO;2-J
Ghosh S, Datta D, Katakdhond AA (2011) Estimation of the Park-Ang damage index for planar multi-storey frames using equivalent single-degree systems. Eng Struct 33:2509–2524
Goel SC, Liao WC, Bayat MR, Chao SH (2010) Performance-based plastic design (PBPD) method for earthquake-resistant structures: an overview. Struct Des Tall Special Build 19:115–137
Kalkan E, Chopra AK (2011) Modal-pushover-based ground-motion scaling procedure. J Struct Eng 137:298–310. https://doi.org/10.1061/(ASCE)ST.1943-541X.0000308
Kent DC, Park R (1971) Flexural members with confined concrete. J Struct Div 97:1969–1990
Kilar V, Fajfar P (1997) Simple push-over analysis of asymmetric buildings. Earthq Eng Struct Dyn 26:233–249. https://doi.org/10.1002/(SICI)1096-9845(199702)26:2%3C233::AID-EQE641%3E3.0.CO;2-A
Kraetzig WB, Meyer IF, Meskouris K (1989) Damage evolution in reinforced concrete members under cyclic loading. Structural safety and reliability 795–804
Kreslin M, Fajfar P (2010) Seismic evaluation of an existing complex RC building. Bull Earthq Eng 8:363–385
Kreslin M, Fajfar P (2011) The extended N2 method taking into account higher mode effects in elevation. Earthq Eng Struct Dyn 40:1571–1589
Kreslin M, Fajfar P (2012) The extended N2 method considering higher mode effects in both plan and elevation. Bull Earthq Eng 10:695–715
Kunnath SK, El-Bahy A, Taylor AW, Stone WC (1997) Cumulative seismic damage of reinforced concrete bridge piers. Technical Report NCEER-97–0006, National Institute of Standards and Technology
Kurama YC, Farrow KT (2003) Ground motion scaling methods for different site conditions and structure characteristics. Earthquake Eng Struct Dynam 32:2425–2450. https://doi.org/10.1002/eqe.335
Leelataviwat S, Goel SC, Stojadinović B (1999) Toward performance-based seismic design of structures. Earthq Spectra 15:435–461
Leelataviwat S, Goel SC, Stojadinović B (2002) Energy-based seismic design of structures using yield mechanism and target drift. J Struct Eng 128:1046–1054
Leelataviwat S, Saewon W, Goel SC (2009) Application of energy balance concept in seismic evaluation of structures. J Struct Eng 135:113–121
Leelataviwat S, Saewon W, Goel SC (2007) An energy-based method for seismic evaluation of structures. In: Proceedings of Structural Engineers Association of California Convention SEAOC, Lake Tahoe, California, USA
Liao WC, Goel SC (2014) Performance-based seismic design of RC SMF using target drift and yield mechanism as performance criteria. Adv Struct Eng 17:529–542
Lin Y, Chang K (2003) An improved capacity spectrum method for ATC-40. Earthq Eng Struct Dyn 32:2013–2025
Mahboubi S, Shiravand MR (2019a) Seismic evaluation of bridge bearings based on damage index. Bull Earthq Eng 17:4269–4297. https://doi.org/10.1007/s10518-019-00614-3
Mahboubi S, Shiravand MR (2019b) Proposed input energy-based damage index for RC bridge piers. J Bridg Eng 24:04018103. https://doi.org/10.1061/(ASCE)BE.1943-5592.0001326
Mazzoni S, McKenna F, Scott MH, Fenves GL (2006) OpenSees command language manual. Pacific Earthquake Engineering Research (PEER) Center. 264:137–158
Miranda E (1993) Evaluation of site-dependent inelastic seismic design spectra. J Struct Eng 119:1319–1338
Miranda E (2000) Inelastic displacement ratios for structures on firm sites. J Struct Eng 126:1150–1159
Miranda E (2001) Estimation of inelastic deformation demands of SDOF systems. J Struct Eng 127:1005–1012. https://doi.org/10.1061/(ASCE)0733-9445(2001)127:9(1005)
Miranda E, Bertero V (1994) Evaluation of strength reduction factors for earthquake-resistant design. Earthq Spectra 10:357–379
Miranda E, Bertero V (1991) Evaluation of structural response factors using ground motions recorded during the Loma Prieta earthquake. CSMIP-1991
Naeim F, Alimoradi A, Pezeshk S (2004) Selection and scaling of ground motion time histories for structural design using genetic algorithms. Earthq Spectra 20:413–426. https://doi.org/10.1193/1.1719028
O'Donnell AP, Kurama YC, Kalkan E et al (2013) Ground motion scaling methods for linear-elastic structures: an integrated experimental and analytical investigation. Earthq Eng Struct Dyn 42:1281–1300. https://doi.org/10.1002/eqe.2272
Panyakapo P (2004) Evaluation of site-dependent constant-damage design spectra for reinforced concrete structures. Earthq Eng Struct Dyn 33:1211–1231
Park YJ, Ang AHS (1985) Mechanistic seismic damage model for reinforced concrete. J Struct Eng (united States) 111:722–739. https://doi.org/10.1061/(ASCE)0733-9445(1985)111:4(722)

Petrini L, Maggi C, Priestley MJN, Calvi GM (2008) Experimental verification of viscous damping modeling for inelastic time history analyzes. J Earthq Eng 12:125–145. https://doi.org/10.1080/13632460801925822

Powell GH, Allahabadi R (1988) Seismic damage prediction by deterministic methods: concepts and procedures. Earthq Eng Struct Dyn 16:719–734. https://doi.org/10.1002/eqe.4290160507

Ruiz-García J, Miranda E (2003) Inelastic displacement ratios for evaluation of existing structures. Earthq Eng Struct Dyn 32:1237–1258

Ruiz-García J, Miranda E (2004) Inelastic displacement ratios for design of structures on soft soils sites. J Struct Eng 130:2051–2061

Ruiz-García J, Miranda E (2006) Inelastic displacement ratios for evaluation of structures built on soft soil sites. Earthq Eng Struct Dyn 35:679–694

Ruiz-García J, Miranda E (2007) Probabilistic estimation of maximum inelastic displacement demands for performance-based design. Earthq Eng Struct Dyn 36:1235–1254

Schoettler MJ, Restrepo JI, Guerrini G, et al (2015) A full-scale, single-column bridge bent tested by shake-table excitation. Pacific Earthquake Engineering Research Center (PEER), University of California, Berkeley, CA, USA

Su J, Dhakal RP, Wang J (2017) Fiber-based damage analysis of reinforced concrete bridge piers. Soil Dyn Earthq Eng 96:13–34. https://doi.org/10.1016/j.soildyn.2017.01.029

Veletsos AS, Newmark NM, Chelapati C v (1965) Deformation spectra for elastic and elastoplastic systems subjected to ground shock and earthquake motions. In: Proceedings of the 3rd world conference on earthquake engineering

Veletsos A, Newmark NM (1960) Effect of inelastic behavior on the response of simple systems to earthquake motions. University of Illinois, Department of Civil Engineering

Wen WP, Zhai CH, Li S et al (2014) Constant damage inelastic displacement ratios for the near-fault pulse-like ground motions. Eng Struct 59:599–607. https://doi.org/10.1016/j.engstruct.2013.11.011

Weng YT, Tsai KC, Chan YR (2010) A ground motion scaling method considering higher-mode effects and structural characteristics. Earthq Spectra 26:841–867. https://doi.org/10.1193/1.3460374

Zarrin M, Gharabaghi ARM, Poursha M (2021) A multi-mode N2 (MN2) pushover procedure for ductility level seismic performance evaluation of jacket type offshore platforms. Ocean Eng 220:108440

Zhai CH, Wen WP, Chen ZQ et al (2013a) Damage spectra for the mainshock-aftershock sequence-type ground motions. Soil Dyn Earthq Eng 45:1–12. https://doi.org/10.1016/j.soildyn.2012.10.001

Zhai CH, Wen WP, Zhu TT et al (2013b) Inelastic displacement ratios for design of structures with constant damage performance. Eng Struct 52:53–63. https://doi.org/10.1016/j.engstruct.2013.02.008

Zhao J, Sritharan S (2007) Modeling of strain penetration effects in fiber-based analysis of reinforced concrete structures. ACI Struct J 104:133. https://doi.org/10.14359/18525